From enhancers to genome conformation: complex transcriptional control underlies expression of a single herpesviral gene

David W Morgens,[1*] Leah Gulyas,[1] Alejandro Rivera-Madera,[2] Annabelle S Souza,[2] Britt A Glaunsinger[1,2,3*]

[1]Department of Plant and Microbial Biology, UC Berkeley, Berkeley, CA, USA; [2]Department of Molecular and Cell Biology, UC Berkeley, CA, USA; [3]Howard Hughes Medical Institute, UC Berkeley, CA, USA

*Corresponding authors: glaunsinger@berkeley.edu, dmorgens@berkeley.edu

Abstract

Complex transcriptional control is a conserved feature of both eukaryotes and the viruses that infect them. Here, we illustrate this by combining high-density functional genomics, expression profiling, and viral-specific chromosome conformation capture to define with unprecedented detail the transcriptional regulation of a single gene, ORF68, from Kaposi's sarcoma-associated herpesvirus (KSHV). We first identified seven cis-regulatory regions by densely tiling the ~154 kb KSHV genome with CRISPRi. A parallel Cas9 nuclease screen indicated that three of these regions act as promoters of genes that regulate ORF68. RNA expression profiling demonstrated that three more of these regions act by either repressing or enhancing other distal viral genes involved in ORF68 transcriptional regulation. Finally, we tracked how the 3D structure of the viral genome changes during its lifecycle, revealing that these enhancing regulatory elements are physically closer to their targets when active, and that disrupting some elements caused large-scale changes to the 3D genome. These data enable us to construct a complete model revealing that the mechanistic diversity of this essential regulatory circuit matches that of human genes.

Introduction

Underlying the lifecycle of all DNA viruses is a highly regulated cascade of viral gene transcription. In human herpesviruses, many of these genes are transcribed in a host-like manner; nuclear dsDNA viral genomes can be chromatinized by human histones,[1] decorated with enhancer marks,[2] driven by human transcription factor binding,[3] and even form transcription-associated domains with human CTCF and cohesion.[4,5] Exhaustively identifying and characterizing these regulatory features can both help us understand the biology of human pathogens such as Kaposi sarcoma-associated herpesvirus (KHSV) – a major cause of cancer in AIDS and other immunocompromised patients – and also contribute to our knowledge of human transcriptional regulation.

Numerous examples of non-coding regulatory sequences have been found in DNA viruses. Enhancer sequences include the first described enhancer on SV40,[6] the EIIA enhancer on adenovirus,[7] the major immediate enhancer element in the betaherpesvirus human cytomegalovirus,[8,9] and a recent proposal that the terminal repeats of KSHV act as enhancers.[10] Other viral regulatory elements act through expression of non-coding elements. In murine gammaherpesvirus 68 there are tRNA-like elements that control latency and egress.[11,12] In KSHV, many different functional elements beyond coding mRNAs are transcribed, including miRNAs that regulate cancer phenotypes,[13,14] origin RNAs that regulate viral DNA replication,[15,16] circular RNAs,[17,18] and long ncRNAs with various functions.[19–23] While these individual events have been explored to different degrees, systematic searches for regulatory sequences have been limited by traditional methods that rely on deletions to perturb noncoding elements, which in the densely encoded KSHV genome may have unintended effects on surrounding elements.

For the human genome, the discovery of functional regulatory sequences has been greatly accelerated by the use of CRISPR interference or CRISPRi.[24–28] Notably, by recruiting repressive chromatin regulators to DNA, CRISPRi can repress gene expression not only through proximal promoter elements but also by perturbing distal, enhancer elements. While this tool has been applied widely on the host, it can also effectively repress transcription from the KSHV genome,[29] and thus has the potential to provide deep insight into the components and structure of viral transcriptional networks. While searches for human regulatory regions are limited to predicted enhancers or nearby regions, the viral regulatory regions will be necessarily contained within the relatively compact viral genome and thus be amenable to exhaustive characterization.

56 Here we combine CRISPRi with a library of guide RNAs densely tiling the KSHV genome, allowing
57 a thorough interrogation of potential regulatory activity controlling the expression of a single viral
58 gene, ORF68. ORF68 was selected as a proof of concept for this study as it has a simple early-
59 expression pattern[30,31] but plays an essential role late in the viral life cycle during packaging of
60 new viral DNA.[32,33] By complementing CRISPRi with a Cas9 nuclease screen and transcriptional
61 profiling, we identified promoters that control expression through their associated coding regions,
62 as well as non-coding regulatory elements that comprise a surprisingly sophisticated network to
63 regulate ORF68 transcription. Finally, we use viral-specific chromosome conformation capture to
64 measure physical interactions between regulatory regions and their distal targets and
65 demonstrate how disruption of these regions changed the 3D structure of the viral genome. These
66 findings illustrate the power of this approach for mapping viral gene regulatory networks on a
67 genome-wide scale.

68

69 **Results**

70 *CRISPRi tiling identifies regulatory regions across the viral genome*

71 We sought to define the layers of regulation underlying the expression of an individual viral gene,
72 using the nuclear replicating dsDNA virus KSHV. We selected KSHV ORF68 as our model gene,
73 as it is required for progeny virion production, has no known direct transcriptional regulators, and
74 its expression initiates early in the lytic cycle and stays on throughout the rest of the viral
75 lifecycle[30,31]. KSHV gene regulation can be readily studied using the renal carcinoma cell line
76 iSLK, a well-established model for the KSHV lifecycle that includes a doxycycline-inducible
77 version of the KSHV lytic transactivator ORF50 to facilitate lytic reactivation from latency.

78 We began construction of this regulatory network by querying how silencing of each KSHV locus
79 using CRISPRi influenced ORF68 expression. We latently infected iSLK cells with a version of
80 KSHV containing a HaloTag fused to the N-terminus of ORF68 at the endogenous locus (HaloTag-
81 ORF68),[34] allowing us to directly measure ORF68 protein levels, as well as a constitutively
82 expressed GFP reporter that marks infected cells. Additionally, we lentivirally introduced a
83 constitutive dCas9-KRAB fusion (CRISPRi), which would be recruited to a targeted viral region
84 upon delivery of a sgRNA. We then delivered a library of guide RNAs densely tiling the KSHV
85 genome with an average of one guide every 8 base pairs.[34] After four days, the virus was
86 reactivated, and cells were treated with a fluorescent HaloTag ligand to monitor ORF68 protein
87 levels. 24 hours post-reactivation, cells were fixed and sorted for high and low ORF68 protein

88 expression (**Figure 1a**). By sequencing the sgRNA locus from both populations, we calculated an
89 average guide enrichment from two replicates. A negative value signifies that the guide was
90 enriched in the low ORF68 signal population, indicating that silencing that locus inhibits the
91 expression of ORF68. Similarly, a positive value signifies that the guide was enriched in the high
92 ORF68 signal population, indicating that silencing that locus increases expression of ORF68
93 (**Figure S1a,b**).

94 We performed a sliding window analysis and identified 8 loci with target guide RNA scores that
95 differed significantly from negative controls (**Figure 1b; Supplementary Data 1, 2**). Our strongest
96 signal corresponded to a peak poised immediately upstream of HaloTag-ORF68 itself, confirming
97 successful transcriptional inhibition of the locus by CRISPRi. We observed that the center of most
98 other peaks also corresponded with known transcriptional start sites (TSSs); since we expect
99 CRISPRi to work primarily by impeding transcription, these peaks are named by their nearest
100 TSS for simplicity (**Figure S1c-h**). For example, we find one peak near the TSS of ALT, a lncRNA
101 of unknown function which runs antisense to many genes expressed during latency,[22] that we will
102 refer to as TSSalt (**Figure S1e**). The exceptions include one peak that roughly maps to the ORF50
103 coding locus (**Figure S1c**) – likely targeting the exogenous copy of ORF50 used to reactivate the
104 virus – as well as an additional peak which does not correspond to a previously described TSS
105 (**Figure S1h**)[35] but is located near the shared polyA sites of ORF75, ORF74, K14, K15, and the
106 ALT lncRNA.[22,36] We will refer to these as ORF50 and polyA75 respectively.

107 We next validated these 8 regions' effect on ORF68 by delivering a pool of three CRISPRi guides
108 per locus and measuring the percentage of cells expressing HaloTag-ORF68 at two timepoints
109 post-reactivation (**Figure 1c**). These confirmed our screen results, but we did note that some of
110 the effects on ORF68 levels were not sustained at later timepoints, most notably when targeting
111 TSSalt. This may reflect changing regulatory events as the viral lifecycle progresses. While guides
112 targeting the EF1a promoter displayed the expected effect as well, these guides were highly toxic,
113 most likely through their association with the BAC-encoded EF1a-EGFP-HygroR selection locus
114 or the possible inhibition of the host EF1a site. Thus, we excluded this peak from further analysis.

115 Despite the correspondence of most peaks to TSSs, the large observed footprint of CRISPRi
116 prevented high resolution identification of important underlying regulatory features. Illustrating
117 this, the TSS68 peak is comprised of guides targeting not only the entirety of the ORF68 coding
118 region, but also many surrounding genes (**Figure 1d**). This equates to approximately a 2-5 kb
119 window of CRISPRi repression from a single guide, which is mirrored at other loci (**Figure S1d**).
120 This large footprint is likely due to the spread of KRAB-induced heterochromatinization[37] and

121 should be taken into account when using sodium butyrate and CRISPRi on viral genomes, which
122 display significantly higher gene density than cellular genomes. This prompted us to further
123 interrogate the global and local transcriptional effects of CRISPRi at each regulatory region on
124 the viral genome.

125

126 *CRISPRi recruitment to the viral genome inhibits many genes locally*

127 The regulatory regions identified above could either impact ORF68 transcription specifically or
128 could more globally disrupt KSHV lytic gene expression. To evaluate these possibilities, we
129 performed polyA+ RNA-seq at 24 hours post-reactivation on the previously validated guide pools
130 (**Figure S2a**). Silencing of the regulatory loci by CRISPRi caused changes in ORF68 mRNA levels
131 that are consistent with those observed at the protein level by both RNA-seq and follow-up RT-
132 qPCR (**Figure 2a, Figure S2b,c, Supplementary Data 3**), suggesting that regulation primarily
133 controls RNA abundance. Nearly all viral genes were downregulated when ORF50, TSS75, or
134 TSS57 were silenced, aligning with the critical roles of ORF50, ORF75, and ORF57 proteins in
135 the viral lifecycle. ORF50 is a master regulator of KSHV lytic reactivation,[38] ORF75 is required to
136 prevent innate immune suppression of viral gene expression,[39,40] and ORF57 has many reported
137 viral functions including the export of viral mRNA from the nucleus.[41]

138 In contrast, guides targeting TSS68 and TSSalt had a limited global effect, strongly inhibiting only
139 a small number of genes each. The strongest downregulated genes fall within the local region of
140 the guides (**Figure 2b,c**), reaffirming that CRISPRi inhibits transcription in region of approximately
141 ~2.5 kb around the targeting site. This appears true even when the effect of CRISPRi increases
142 ORF68 mRNA expression, as in the case of TSS72. Silencing the TSS72 region causes a global
143 increase in viral gene expression (**Figure 2a**) despite still locally decreasing transcription (**Figure**
144 **2d**). Many of these locally repressed regions include ORF73, which encodes for LANA, whose
145 expression is required for latency maintenance,[3,42] though whose knockdown was not seen here
146 to affect ORF68 expression. To test whether targeting TSS72 is affecting latency, we grew our
147 knockdown lines in the absence of hygromycin selection and observed a more rapid loss of
148 latency only when targeting TSS75 or polyA75 (**Figure S2d**). Thus, RNA-seq corroborates our
149 screening data, and reveals both local and global effects of CRISPRi at our target loci.

150 We next tested whether these altered ORF68 and ORF75 RNA levels stem from transcriptional
151 changes after CRISPRi targeting of the regulatory loci. At 24 hours post reactivation, we used
152 ethynyl uridine (EU) to metabolically label newly transcribed RNA for two hours. EU-labeled RNA

153 was purified, modified with biotin, and isolated, and the levels of newly synthesized ORF68 and
154 ORF75 mRNA were measured by RT-qPCR (**Figure 2e**). As expected, targeting TSS68 or TSS75
155 had a dramatic effect on their respective nascent RNAs, and silencing of other regulatory loci
156 yielded a reduction or increase in EU-labeled RNA consistent with total RNA levels. The exception
157 is TSS57, whose silencing did not significantly reduce nascent ORF68 mRNA at 24 hours post
158 reactivation. Thus, while these regulatory loci all impact the total RNA abundance of their targets,
159 they may do so through a combination of transcriptional and post-transcriptional mechanisms.

160

161 *Viral knockouts identify associated coding features*

162 While CRISPRi at a given locus may effectively suppress multiple viral genes, not every gene will
163 be responsible for the observed effect on ORF68 expression. For example, while guides targeting
164 the TSS68 repress expression of ORFs 65, 66, 67, 68, and 69 (**Figure 2b**), downregulation of the
165 ORF68 reporter is most likely due to direct repression of the ORF68 promoter. Furthermore,
166 CRISPRi alone is unable to distinguish whether regulatory regions influence transcription of a
167 regulatory protein or act by a non-coding mechanism. Therefore, we next directly assessed the
168 role of coding loci underlying each regulatory locus by performing a CRISPR nuclease tiling
169 screen, using a version of the HaloTag-ORF68 reporter iSLK line containing Cas9 instead of
170 CRISPRi.

171 In previous screens, we have reported a strong background effect, where targeting any locus on
172 the viral genome with Cas9 nuclease resulted in a decrease in reporter expression.[34] Here, we
173 observed unexpectedly that this background effect was variable across the viral genome, with
174 targeting to the region upstream of the ORF68 coding region having a stronger effect on reporter
175 expression than targeting downstream (**Figure S3a, Supplementary Data 4,5**). The reason for
176 this difference is unknown (possibly a local effect of DNA damage on the viral genome), but to
177 adjust for the differences in local background we used a boundary method to identify coding
178 regions: for each candidate coding exon, we compared the enrichment of the coding region to the
179 immediate adjacent non-coding region, and considered the coding region a hit if the boundaries
180 were both significantly increased or both significantly decreased.

181 This yielded an exhaustive list of viral coding regions that control ORF68 expression at 24 hours
182 post-reactivation: ORF50, HygroR, ORF68, and ORF75 (**Figure 3a-c; Figure S3b**). Targeting the
183 corresponding CRISPRi loci of ORF50, TSS68, and TSS75 each disrupt ORF68 expression, while
184 CRISPRi repression of the EF1a promoter controlling HygroR expression increased ORF68

185 expression. Loss of functional protein thus likely explains these regions' effect on ORF68. In
186 contrast, we observe no effect on ORF68 of targeting ORF57 and ORF72 coding regions with
187 Cas9 (**Figure S3c,d**). Thus, TSS57 and TSS72 presumably impact ORF68 independently of their
188 associated coding ORFs. The final two CRISPRi loci, TSSalt and PolyA75, are not located at the
189 promoters of any coding regions, and indeed we find no evidence of a coding region near TSSalt
190 that affected ORF68 expression. PolyA75 is adjacent to the ORF75 coding locus, but no other
191 coding elements are identified that could explain its activity. These regions with no associated
192 coding region thus likely act through noncoding elements that are unable to be efficiently disrupted
193 by Cas9.

194 To test whether the identified coding regions have the expected negative effect on the mRNA
195 levels of ORF68, we cloned pooled guides for nuclease-targeting at the coding regions of ORF50
196 and ORF75, including ORF57 as a negative control. ORF50 and ORF75 pools had the expected
197 effect of decreasing ORF68 protein levels (**Figure 3d**) as well as corresponding depletion of
198 ORF68 RNA (**Figure 3e**). To determine whether ORF50 and ORF75 are direct or indirect
199 activators of ORF68, we transfected a reporter plasmid containing 230 bp of upstream of the
200 ORF68 start codon driving a HaloTag reporter along with an expression plasmid of either ORF50
201 or ORF75 into HEK293T cells. Only ORF75 caused a significant increase in expression from the
202 ORF68 promoter (**Figure 3f**). Given that ORF50 is required for ORF75 expression (**Figure 3e**),
203 these data suggest a regulatory model of protein coding elements where ORF50 activates ORF75
204 which, in turn, activates ORF68. We also observed that targeting either ORF50 or ORF75 reduced
205 RNA levels of ORF57 (**Figure 3e**). Interestingly, sgORF57 pools reciprocally decreased ORF75
206 RNA levels, yet ORF57 protein disruption had little or no effect on ORF68 mRNA levels – as
207 predicted by the nuclease screen – suggesting an unclear regulatory relationship.

208

209 *Mapping regulatory targets of noncoding elements*

210 The remaining CRISPRi peaks at TSS57, TSSalt, TSS72, and polyA75 presumably are noncoding
211 loci that instead act in a distal manner to indirectly impact one of the three viral proteins that affect
212 ORF68 expression. We therefore returned to our RNA-seq data and measured the correlation
213 between each sample (**Figure 4a**). We hypothesized that despite local effects of CRISPRi, the
214 regulatory regions would correlate most strongly with their regulatory target, and as we have
215 identified all regulatory regions the number of potential targets is limited. TSSalt and polyA75 most
216 strongly correlated with TSS68 and TSS75 respectively, suggesting that these regions promote

217 ORF68 and ORF75 expression. Conversely, TSS72 had a strong anticorrelation with polyA75 and
218 TSS75. Given that recruitment of CRISPRi to TSS72 causes an increase in viral gene expression,
219 this suggests that TSS72 acts to repress expression of ORF75. TSS57 weakly correlated with
220 many targets, preventing any firm conclusion. We can thus use these correlative regulatory
221 interactions along with data from **Figure 3** to create a model regulatory network consisting of both
222 coding and non-coding elements controlling ORF68 expression (**Figure 4b**). Of note, as we
223 performed these experiments while overexpressing ORF50 from an exogenous promoter, we
224 were likely unable to detect any regulation of the viral copy of ORF50. While silencing TSS57,
225 ORF57, or TSSalt each decreased transcription of ORF75 (**Figure 2e,f; Figure 3e**), we have
226 excluded these interactions from our model as we did not observe the expected subsequent
227 changes to global or ORF68 transcription (**Figure 2a**).

228 To test this model, we evaluated how the components of this ORF68 regulatory network impacted
229 virion production in KSHV infected cells using a supernatant transfer assay. BAC16 derived KSHV
230 expresses GFP, which enables quantification of infected recipient HEK293T cells by flow
231 cytometry. As expected, targeting any of the coding elements via their promoters (TSS57, TSS68,
232 TSS75) caused a severe loss in infectious virion production (**Figure 4c**). Targeting polyA75 also
233 reduced virion production, albeit more modestly, consistent with the regulatory network. In
234 contrast, guides targeting TSS72 or TSSalt did not negatively impact virion production (**Figure**
235 **4c**). This was expected for TSS72, whose silencing increases ORF68 expression. However, that
236 targeting TSSalt – which specifically disrupts ORF68 expression at the early 24h but not the late
237 48h late time point (see **Figure 1c**) – did not impair virion production suggests that while ORF68
238 expression is essential late in infection, it may be dispensable at early time points.

239

240 *Physical interactions of noncoding regions and their targets*

241 We hypothesized that these noncoding elements at TSSalt, TSS72, and polyA75 function distally
242 as either enhancers or regulators of the 3D viral genome structure. Enhancers are expected to
243 be physically close to their target promoters, which can be determined by measuring genome
244 architecture using chromosome capture techniques like Hi-C. Previous work has demonstrated
245 that high-quality viral-viral or viral-host contacts can be obtained using capture Hi-C.[5,43,44] We thus
246 evaluated this approach on iSLK-BAC16 cells 24 hours post reactivation (**Figure 5a;**
247 **Supplementary Data 7**). Indeed, by applying KSHV-specific sequence capture to our libraries,
248 we were able achieve high (<2 kb) resolution contact frequency maps on the viral genome (**Figure**

249 **S5a**) with relatively few sequencing reads (~7 million reads). Contact features were clear at 1-2
250 kb resolution but still notable at even higher (500 bp) resolution (**Figure S5a**).

251 We first asked whether the regulatory elements that interact functionally are also physically
252 proximal, which would be consistent with their activity as enhancers. To function as an enhancer,
253 TSSalt should have a high contact frequency with its target TSS68, while TSS72 and polyA75
254 should have a high contact frequency with their target TSS75. Indeed, this is the case: when
255 looking at the contact frequency of these regions with the rest of the viral genome at 1 kb
256 resolution, TSSalt, TSS72 and polyA75 are physically close to their identified targets but not to
257 another regulator region, TSS57 (**Figure 5b,5c**). This also holds true in the reciprocal interactions
258 (**Figure S5b-d**). These results are consistent with TSSalt, TSS72, and polyA75 functioning as
259 enhancers and exclude the possibility that TSS57 itself is acting as an enhancer targeting either
260 TSS68 or TSS75.

261 We next asked whether this physical proximity is greater than would be expected given the linear
262 genomic distance between the elements and their regulatory targets. Previous Hi-C data has
263 consistently identified that contact frequency is reduced with distance and that this decay can be
264 modeled using a power law.[45,46] However, the relationship between linear distance and the
265 observed contact frequency on the viral genome diverged at higher distances (**Figure S5e**),
266 presumably reflecting that the KSHV genome is present in circular and concatenated forms.[43]
267 Indeed, a distance metric adjusted for these forms better matched the power law expectation
268 (**Figure S5f**) and was used for subsequent analyses.

269 By normalizing the measured contact frequencies (**Figure S5a**) to the expected contact frequency
270 based on distance, we obtained a relative contact frequency that represents the structure of the
271 viral genome at 1 kb resolution (**Figure 5d**). In agreement with the close contacts shown in **Figure**
272 **5b-c**, we observed a strongly associated region from ~129-154 kb that contains TSS68, TSSalt,
273 TSS72, polyA75, and TSS75 (**Figure 5d, outlined region 1**), indicating that these regulatory
274 elements are physically closer than expected given their linear distance. Of note, this corresponds
275 to the region with increased background in the Cas9 screen (**Figure S3a**), consistent with
276 disruptions to this region causing changes to local transcription. Compartments like this exist on
277 the KSHV genome at a smaller scale than typical transcriptional-associated domains (TADs),[43]
278 so we instead refer to them as insulated regions. Other stand-out physical associations include
279 the 129-154 kb insulated region and the 1-3 kb region containing promoters for K1, ORF4, and
280 ORF6 (**Figure 5d, region 2**), as well as the region around TSSalt (which includes the right lytic
281 origin of replication), and region at ~24 kb which includes the left lytic origin of replication (**Figure**

282 **5d, region 3**). These physical associations may represent chromosomal loops between distal
283 regions of the viral genome. However, evaluating whether these loops are statistically significant
284 or if there are additional loops present would require a robust statistic, and it is unclear what would
285 be appropriate given the small size of the viral genome, the high frequency of distal interactions,
286 and the irregular shape of the loops we do see.

287

288 *Changing physical relationship between regulatory regions*

289 If ongoing transcription at these regulatory elements is important for physical interaction with their
290 targets, we reasoned that silencing them could alter the architecture of the viral genome. We
291 tested this by targeting each regulatory element using CRISPRi, then performing capture Hi-C to
292 measure how the 3D structure of the viral genome changed. We modeled how the genome
293 structure changes by grouping the resulting capture Hi-C maps into initial, intermediate, and final
294 stages, representing progression through the viral lytic lifecycle and the regulatory network
295 controlling ORF68 expression by introducing a roadblock caused by silencing each element
296 (**Figure 6a; Supplementary Data 7**). Maps from unreactivated cells and reactivated cells with
297 silenced ORF50 (sgORF50) represented the initial stage, as the viral lytic cycle cannot progress
298 in the absence of ORF50. The intermediate stage comprised the maps from reactivated cells with
299 silenced TSS75, TSS57, and PolyA75, as the RNA-seq data indicated these cause significant
300 changes to the viral transcriptome. The final stage comprised the maps from cells with silenced
301 TSS68, TSSalt, the negative control vSAFE, and the negative regulatory element TSS72.

302 We first examined the insulated region at 129-154 kb, which contains many of these regulatory
303 elements. At 1 kb resolution, we observed large structural changes to this region as the viral life
304 cycle progresses from the initial (**Figure 6b**) to the intermediate (**Figure 6c**) to the final stage
305 (**Figure 6d**), with this 129-154 kb compartment only clearly forming in the final stage. We
306 quantitatively assessed these structures using an insulator score, which was calculated from the
307 relative frequency of contacts across a given region. Insulators "protect" expressing genes from
308 the neighboring genomic environment; they were thus detected here as areas with fewer than
309 expected contacts that span the region, i.e., a low insulator score. These values showed strong
310 concordance within each stage at 2 kb resolution (**Figure S6a-c**), and we used them to visualize
311 compartments by defining their surrounding insulator boundaries as regions with locally minimum
312 insulator scores across the viral genome (**Figure 6e,f,g)**. These results are consistent with
313 previous work demonstrating that the KSHV genome is highly structured before and after

314 reactivation.[43,47–49] However, we note that the insulator strength in the final stage is globally
315 reduced (**Figure S6c**), supporting reduced chromatinization of the viral genome in later stages of
316 the lytic cycle.[2] We did not observe any large shifts in 3D structures when silencing polyA75,
317 TSSalt, or TSS72 when compared to other targets in their stages (**Figure S6d-f**), suggesting they
318 only regulate the 3D genome structure via their regulatory targets.

319 In addition to observing changes in the compartment structure between stages, we also quantified
320 the strength of the insulators at a given region that separates these compartments. As the
321 regulatory circuit progresses, there is a weakening of the insulator at 100-102 kb, an appearance
322 of an insulator at 128-130 kb, and the loss of an insulator at 136-138 kb (**Figure 6h-j**). This
323 corresponds to the region at 128-138 kb moving from a compartment at 100-130 kb to form the
324 ~129-154 kb insulated region we originally noted (**Figure 5d**). As this region contains ORF68, we
325 next asked how these changes affect the contact frequency between the regulatory elements and
326 their targets. While we do not see any large shifts in the physical interactions of the ORF72 locus
327 with TSS75 relative to the reactivated control (**Figure 6g**), the interaction between polyA75 and
328 TSS75 is stronger in both the initial and intermediate stages (**Figure 6h**). This is consistent with
329 our functional data showing that targeting polyA75 reduces ORF75 function even before
330 reactivation (**Figure S2d**) and may represent a dilution of the interactions as the insulator at 136-
331 138 kb is lost (**Figure 6j**) and the compartment containing polyA75 and TSS75 is expanded
332 (**Figure 6f,g**). In contrast, we find that TSSalt and TSS68 are farther apart when targeting either
333 TSS75 or TSS57 (**Figure S6i**), suggesting that this regulatory interaction is inhibited when
334 silencing these regions. While TSS75 likely also acts directly on TSS68 via the ORF75 protein
335 (**Figure 3f**), this allows us to complete the regulatory network by incorporating the effect of
336 targeting TSS57 on the interaction between TSS68 and TSSalt (**Figure S6j**). Thus, by silencing
337 individual regulatory elements and performing capture Hi-C, we determined how each element
338 contributes to the 3D structure of the viral genome; by further incorporating the model for ORF68
339 transcriptional regulation, we also mapped the 3D changes to the genome as the viral lifecycle
340 progressed.

341

342 **Discussion**

343 Here, we identified novel regulatory events across the KSHV genome that control the expression
344 of ORF68 and were able distinguish between coding and noncoding elements, identify their
345 regulatory targets, and establish their changing physical relationships in the 3D genome. Like

346 many other viral early genes, ORF68 has a simple expression pattern: it turns on early in the lytic
347 cycle and remains on throughout. In this light, the model regulatory network we built – and
348 characterized through exhaustive functional genomics, transcriptional profiling, and capture Hi-C
349 – is surprisingly complex. The virus borrows widely from the regulatory toolbox of its human host,
350 spanning promoters, enhancers, repressors, and 3D structural elements. However, unlike the
351 host, all these elements are contained within a compact, densely encoded genome, allowing us
352 to identify a near-complete architecture controlling gene expression within the human nucleus.

353 Our functional model does not make predictions for the mechanistic nature of all these regulatory
354 events. For example, the coding elements may or may not directly regulate transcription on the
355 viral genome. Indeed, whereas ORF50 has been previously characterized as a viral transcription
356 factor,[38,50] ORF75 more likely acts indirectly by preventing inhibition of viral transcription by host
357 factors.[51] Similarly, the non-coding elements could involve ncRNAs, microRNAs, or enhancers,
358 as CRISPRi is expected to be able to inhibit each of these; though as we see a direct effect on
359 transcription (**Figure 2b)** and physical proximity between regulatory region and target (**Figure 5**),
360 we favor an enhancer model. Given the density of the viral genome and the width of CRISPRi
361 footprint, it is possible a peak corresponds to multiple regulatory events or that two nearby peaks
362 both inhibit the same regulatory locus. The TSSalt here could be an example of the former, as
363 there are nearby K12 TSS and miRNA loci (**Figure S1e**), and indeed a recent investigation has
364 proposed that two distinct sequences here have regulatory activity.[52] The polyA75 peak could be
365 an example of the latter as it behaves very similarly to the nearby TSS75 peak. Though with the
366 viral density and propensity for multiple functions encoded within the same locus, these issues
367 may be intrinsic to the study of gene regulation on the viral genome, but it is possible that other
368 functional perturbations such as using base editors or dCas9 could allow us to pinpoint the
369 underlying regulatory sequence.

370 It is also difficult to distinguish the effects of disrupting ORF57 protein and the regulatory element
371 at TSS57. Our observation that Cas9-based disruption of ORF57 did not affect ORF68 mRNA or
372 protein suggests that ORF57 protein does not regulate ORF68. This is in agreement with previous
373 reports using an ORF57 deletion virus, which also indicated little regulatory effect on ORF68.[53]
374 ORF57 protein does have a broad effect on viral transcription, but this is likely through direct
375 effects on DNA replication components, upon which the majority (but not ORF68[30]) of gene
376 expression is partially dependent. It is possible that the TSS57 promoter contributes to ORF68
377 regulation independent from the ORF57 protein, as many human promoters act as enhancers for
378 distal genes,[54] but we do not observe a physical association between TSS57 and either TSS75

379 or TSS68 (**Figure 5b,c**). Instead, we see that targeting TSS57 causes a large disruption to the
380 3D conformation of the KSHV genome (**Figure 6c**), leading to a reduced interaction between
381 TSSalt and TSS68 (**Figure S6i**), potentially disrupting this enhancer-promoter relationship.
382 However, this remains a hypothesis as we cannot disrupt the promoter and its hypothetical
383 structural activity using CRISPRi without also disrupting the protein levels of ORF57.

384 Our approach demonstrates the power of combining CRISPR screening tools for the discovery of
385 viral gene regulatory networks. Given that KSHV is a nuclear double-stranded DNA virus, it
386 incorporates the same spectrum of regulatory mechanisms as the host – transcription factors,
387 non-coding RNAs, enhancers, and DNA structural elements. By studying these networks on the
388 viral genome, we can thus learn both how these regulatory mechanisms function and, ultimately,
389 how the virus controls gene expression under diverse cellular conditions and in various cell types.

390

Figure 1

A

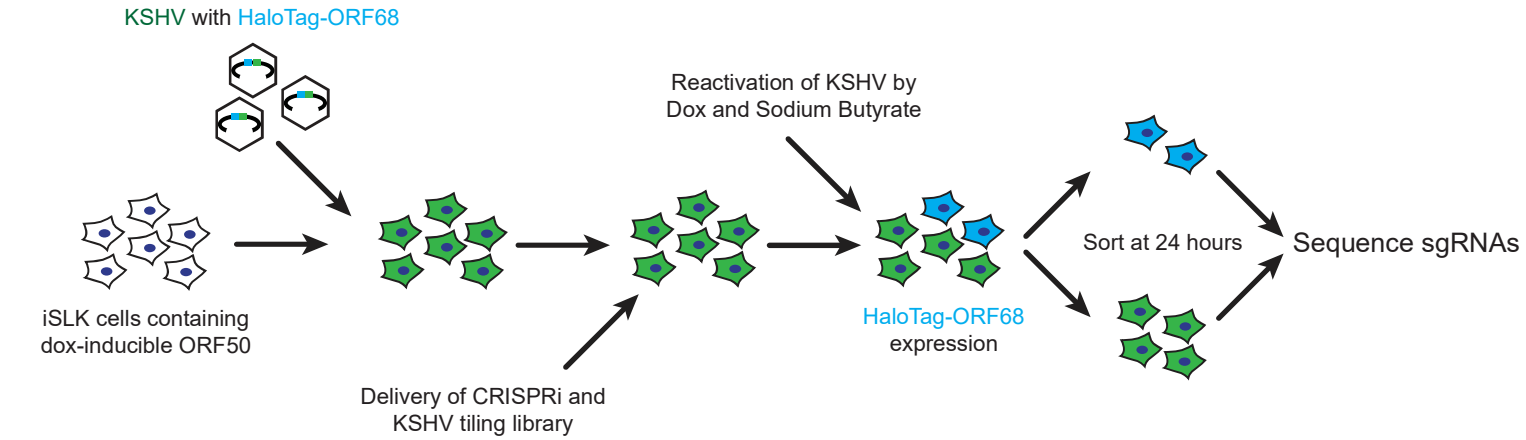

B

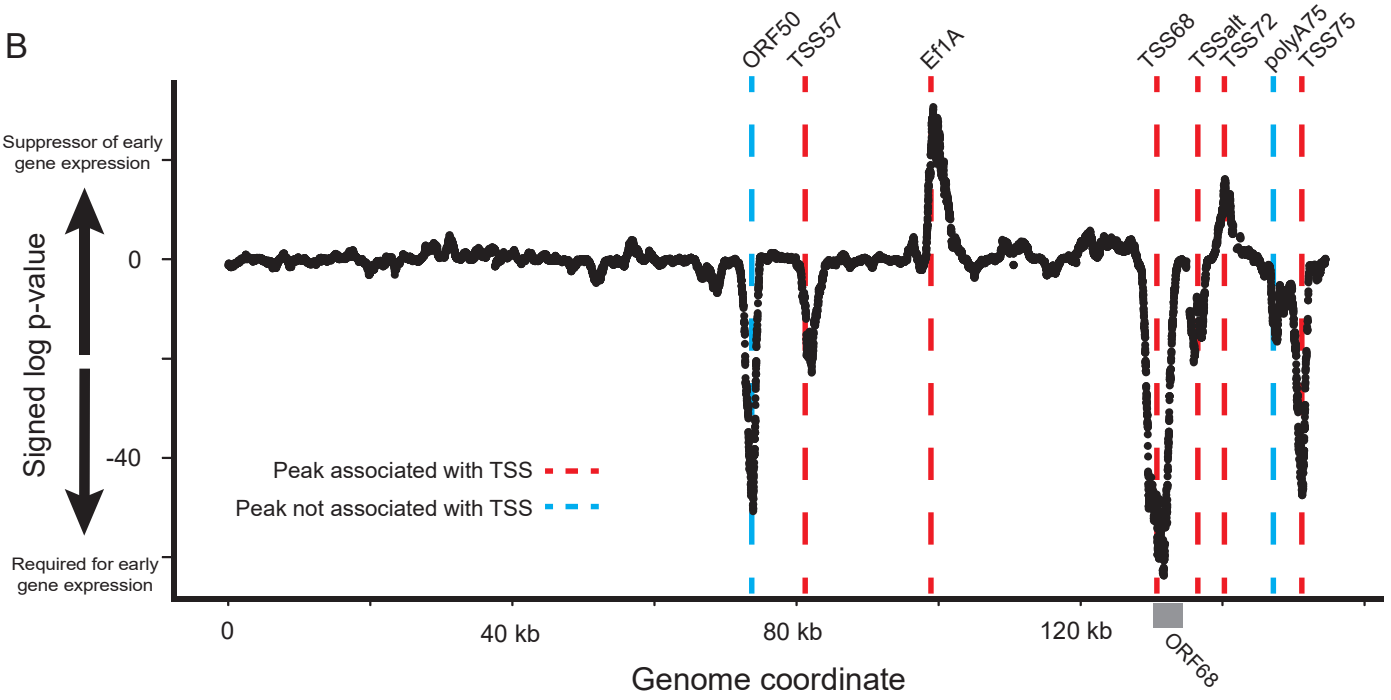

C

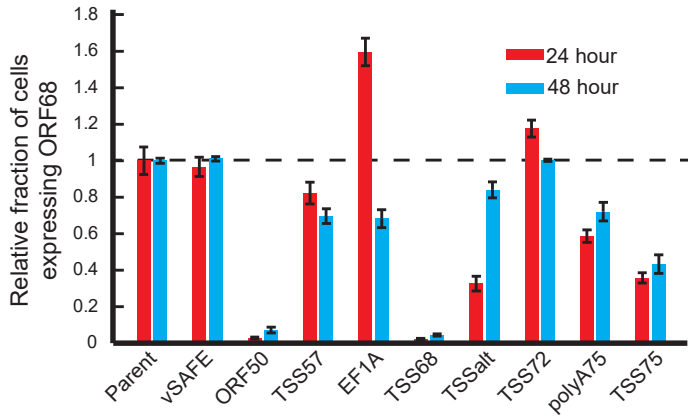

D

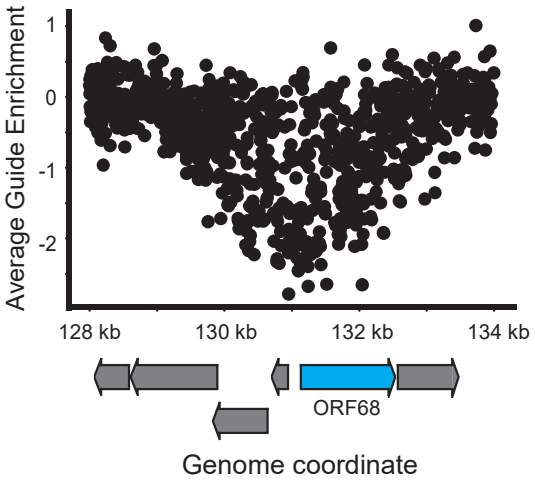

Figure S1

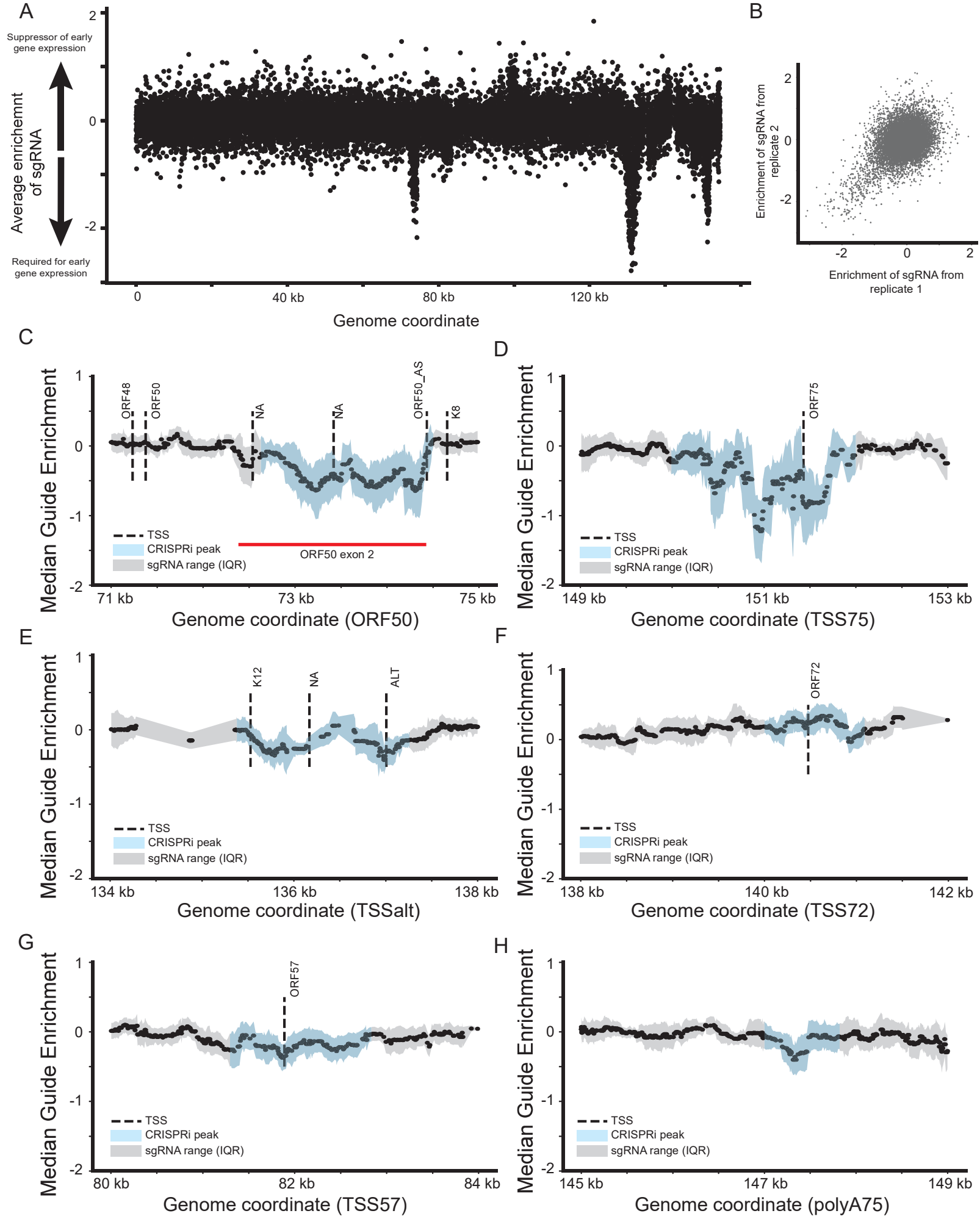
A
Suppressor of early gene expression
Average enrichemnt of sgRNA
Required for early gene expression
2
0
-2
0
40 kb
80 kb
120 kb
Genome coordinate
B
Enrichment of sgRNA from replicate 2
Enrichment of sgRNA from replicate 1
C
Median Guide Enrichment
ORF48
ORF50
NA
NA
ORF50_AS
K8
TSS
CRISPRi peak
sgRNA range (IQR)
ORF50 exon 2
71 kb
73 kb
75 kb
Genome coordinate (ORF50)
D
ORF75
149 kb
151 kb
153 kb
Genome coordinate (TSS75)
E
K12
NA
ALT
134 kb
136 kb
138 kb
Genome coordinate (TSSalt)
F
ORF72
138 kb
140 kb
142 kb
Genome coordinate (TSS72)
G
ORF57
80 kb
82 kb
84 kb
Genome coordinate (TSS57)
H
145 kb
147 kb
149 kb
Genome coordinate (polyA75)

Figure 2

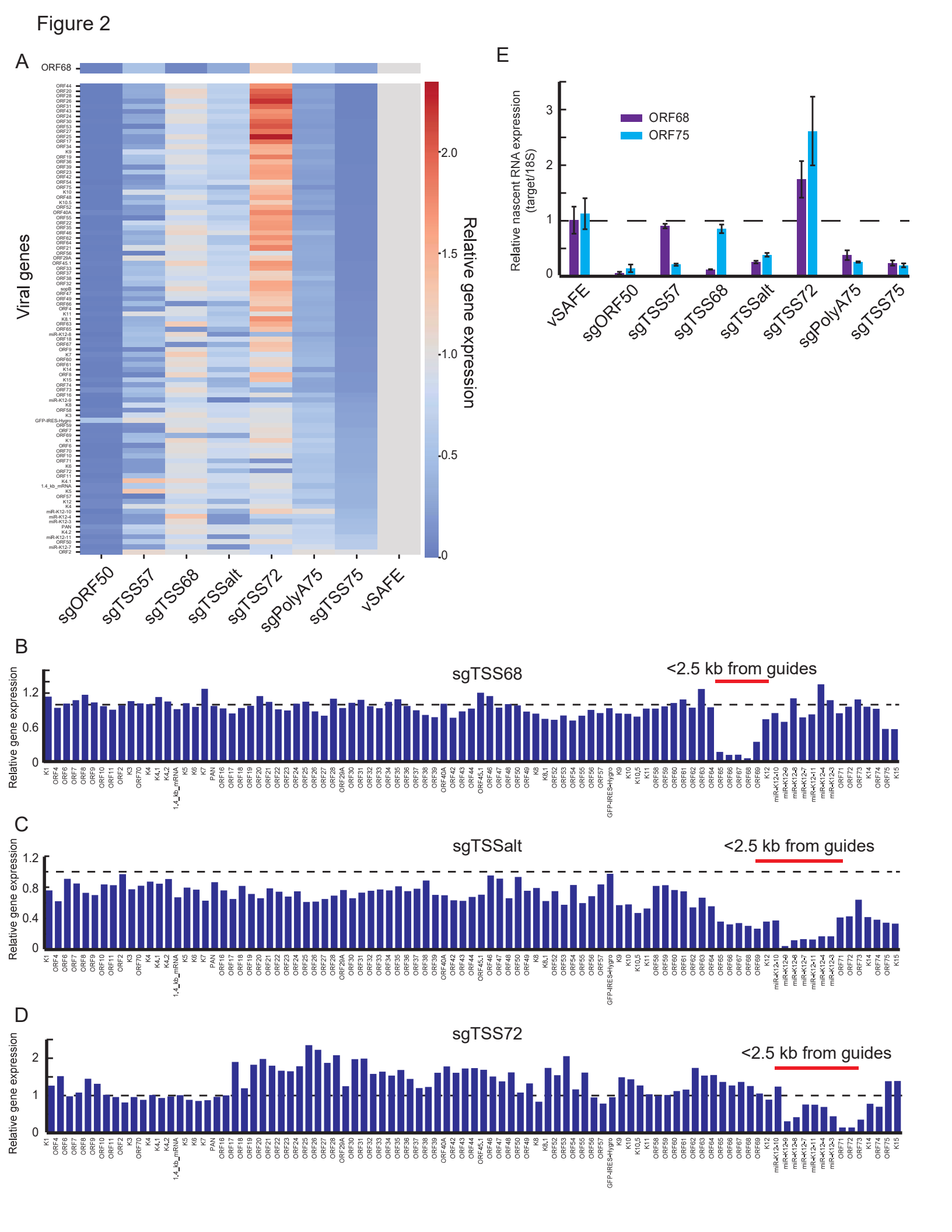
A
ORF68
Viral genes
Relative gene expression
2.0
1.5
1.0
0.5
0
sgORF50
sgTSS57
sgTSS68
sgTSSalt
sgTSS72
sgPolyA75
sgTSS75
vSAFE
E
Relative nascent RNA expression (target/18S)
ORF68
ORF75
3
2
1
0
vSAFE
sgORF50
sgTSS57
sgTSS68
sgTSSalt
sgTSS72
sgPolyA75
sgTSS75
B
sgTSS68
<2.5 kb from guides
Relative gene expression
1.2
0.6
0
C
sgTSSalt
<2.5 kb from guides
Relative gene expression
1.2
0.8
0.4
0
D
sgTSS72
<2.5 kb from guides
Relative gene expression
2
1
0

Figure S2

A

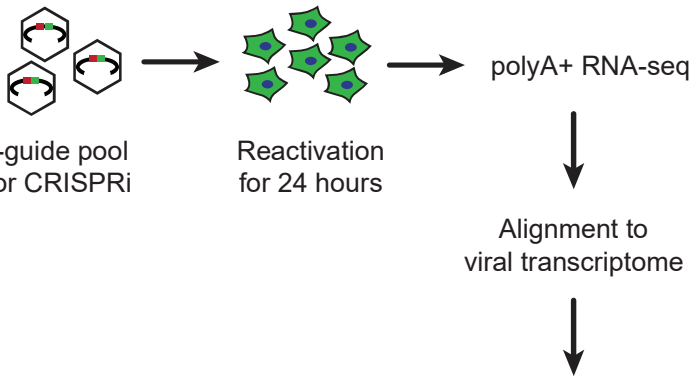

Global effects: How does silencing regulatory elements affect transcription across the viral genome? (Figure 2a)
Local effects: How does transcription change immediately adjacent to the targeted site? (Figure 2b-d)
Correlation: Which regulatory elements have similiar global effects on viral transcription when silenced? (Figure 4a)

B

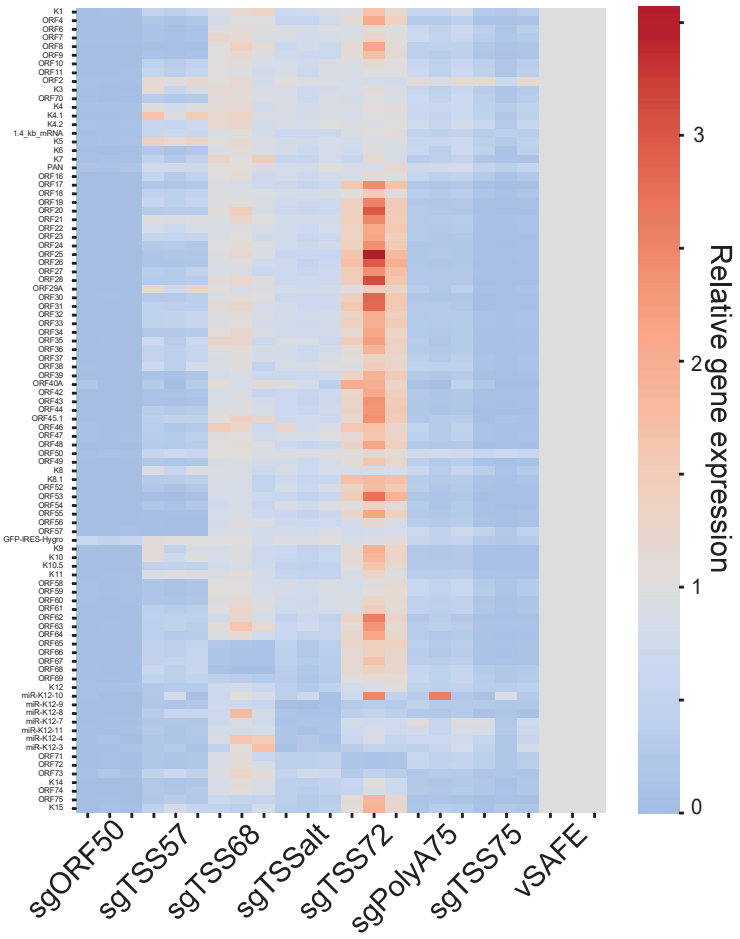

C

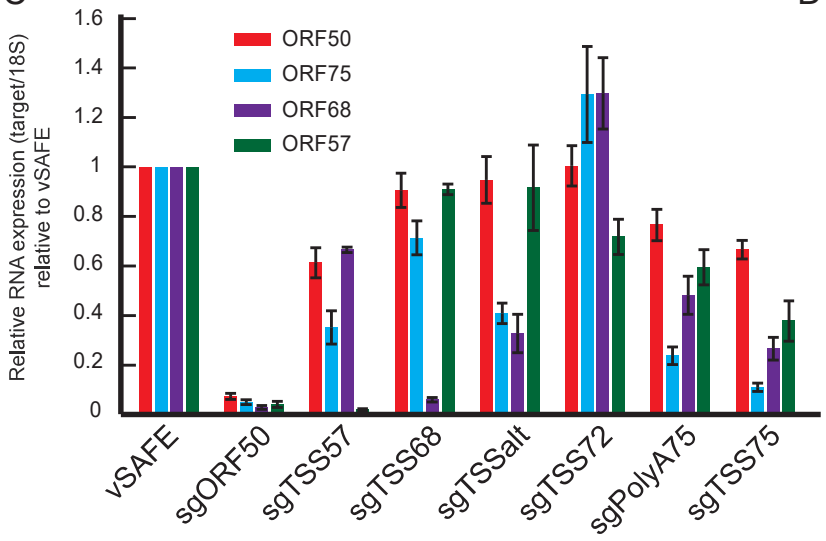

D

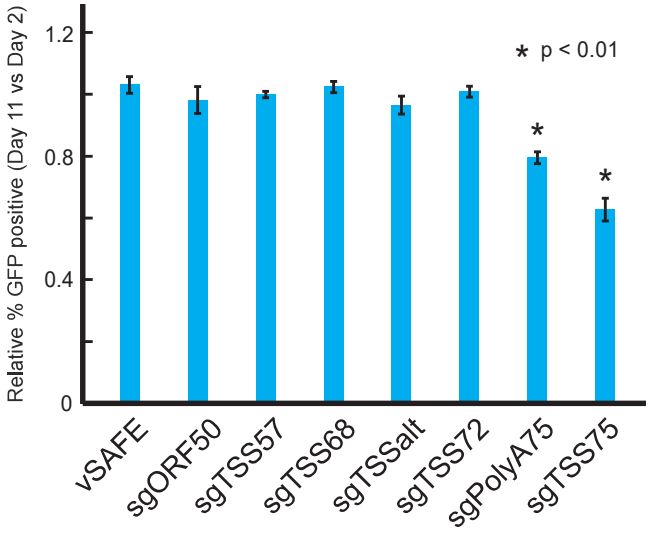

Figure 3

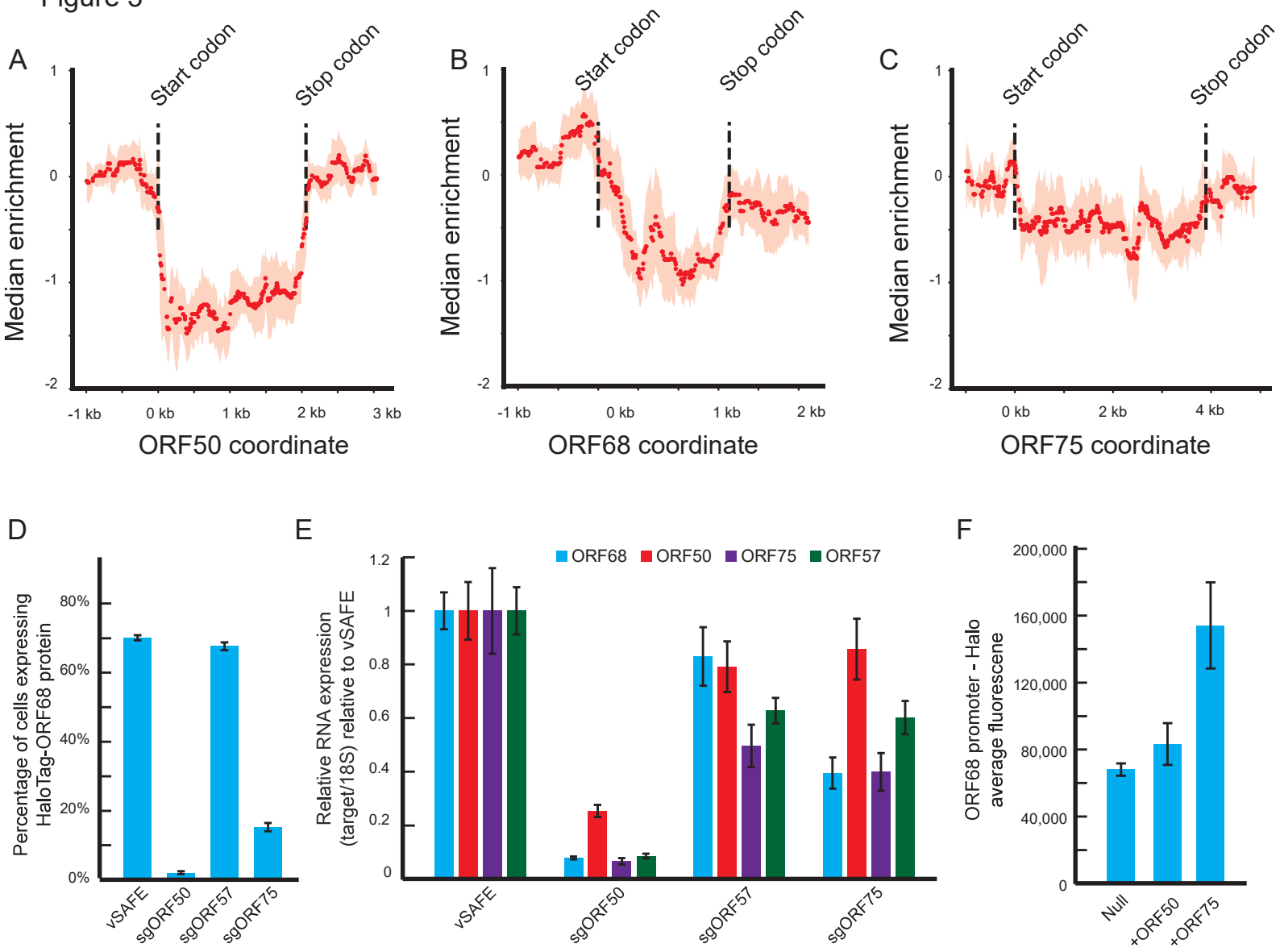
A
Start codon
Stop codon
Median enrichment
1
0
-1
-2
-1 kb
0 kb
1 kb
2 kb
3 kb
ORF50 coordinate
B
Start codon
Stop codon
Median enrichment
1
0
-1
-2
-1 kb
0 kb
1 kb
2 kb
ORF68 coordinate
C
Start codon
Stop codon
Median enrichment
1
0
-1
-2
0 kb
2 kb
4 kb
ORF75 coordinate
D
Percentage of cells expressing HaloTag-ORF68 protein
80%
60%
40%
20%
0%
vSAFE
sgORF50
sgORF57
sgORF75
E
ORF68
ORF50
ORF75
ORF57
Relative RNA expression (target/18S) relative to vSAFE
1.2
1
0.8
0.6
0.4
0.2
0
vSAFE
sgORF50
sgORF57
sgORF75
F
ORF68 promoter - Halo average fluorescene
200,000
160,000
120,000
80,000
40,000
0
Null
+ORF50
+ORF75

Figure S3

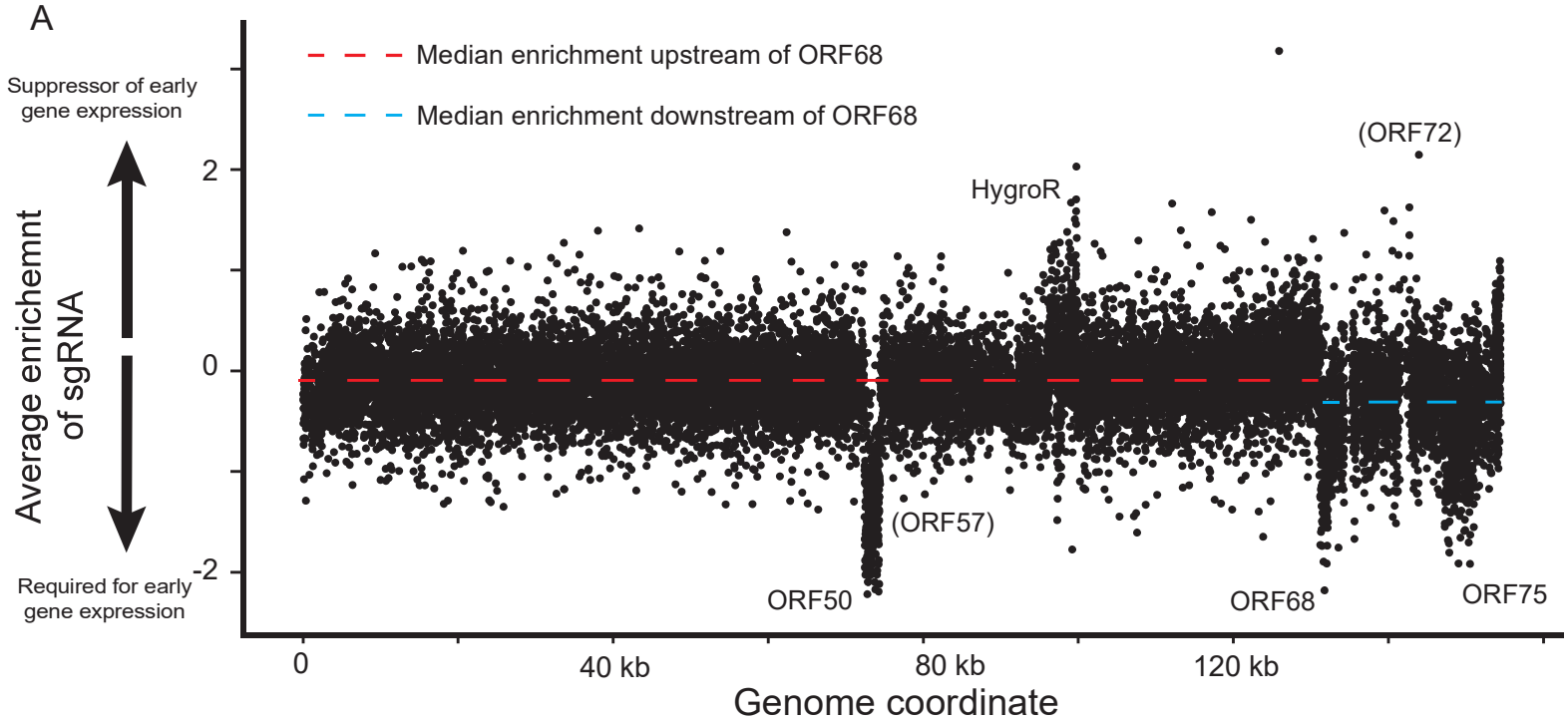
A
Median enrichment upstream of ORF68
Median enrichment downstream of ORF68
Suppressor of early gene expression
Required for early gene expression
Average enrichemnt of sgRNA
2
0
-2
HygroR
(ORF72)
(ORF57)
ORF50
ORF68
ORF75
0
40 kb
80 kb
120 kb
Genome coordinate

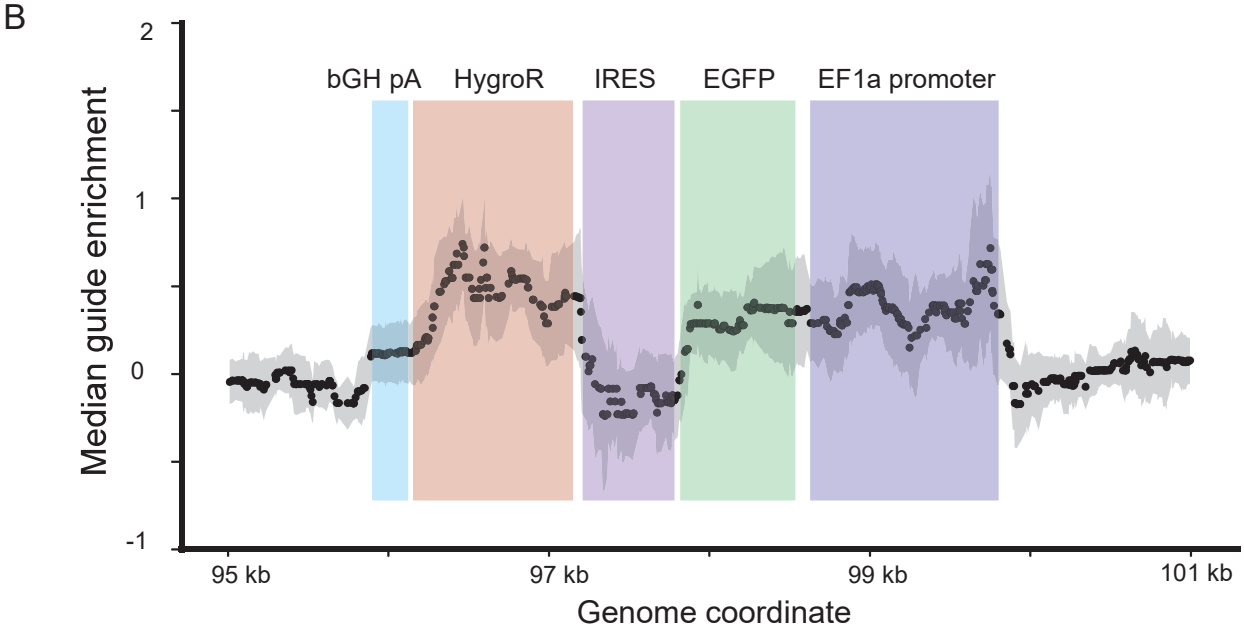
B
bGH pA
HygroR
IRES
EGFP
EF1a promoter
Median guide enrichment
2
1
0
-1
95 kb
97 kb
99 kb
101 kb
Genome coordinate

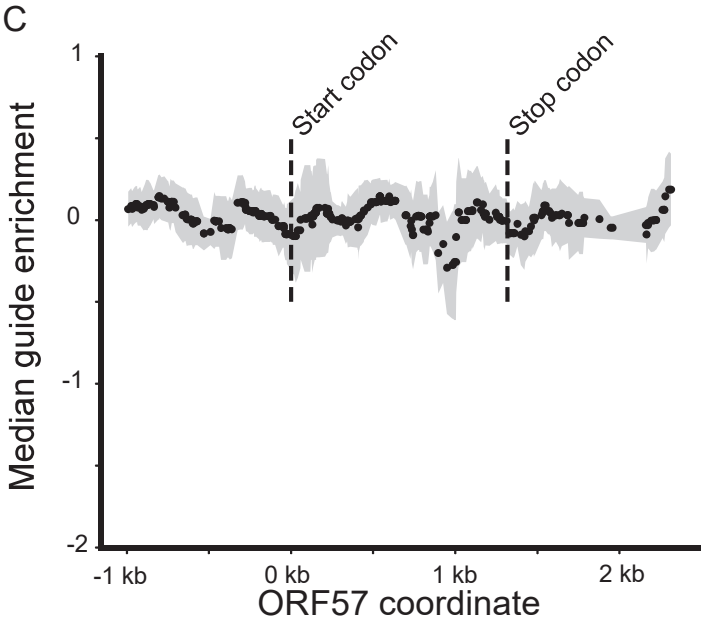
C
Start codon
Stop codon
Median guide enrichment
1
0
-1
-2
-1 kb
0 kb
1 kb
2 kb
ORF57 coordinate

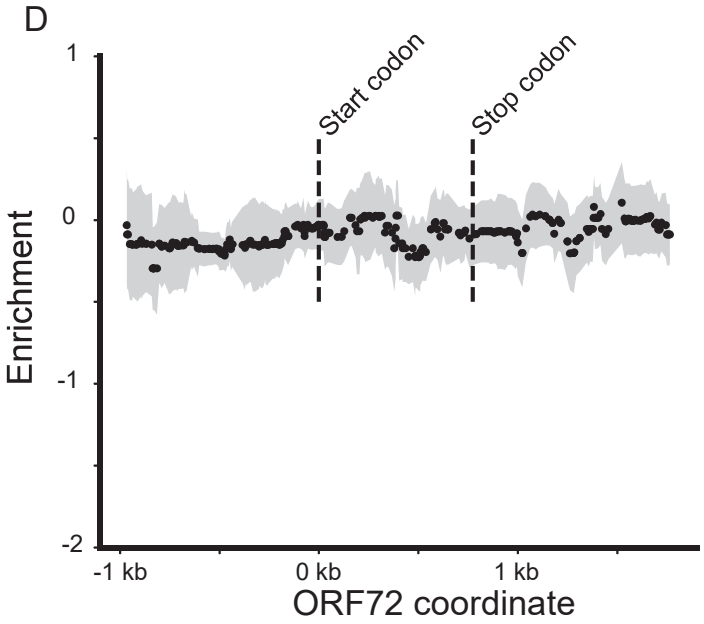
D
Start codon
Stop codon
Enrichment
1
0
-1
-2
-1 kb
0 kb
1 kb
ORF72 coordinate

Figure 4

A

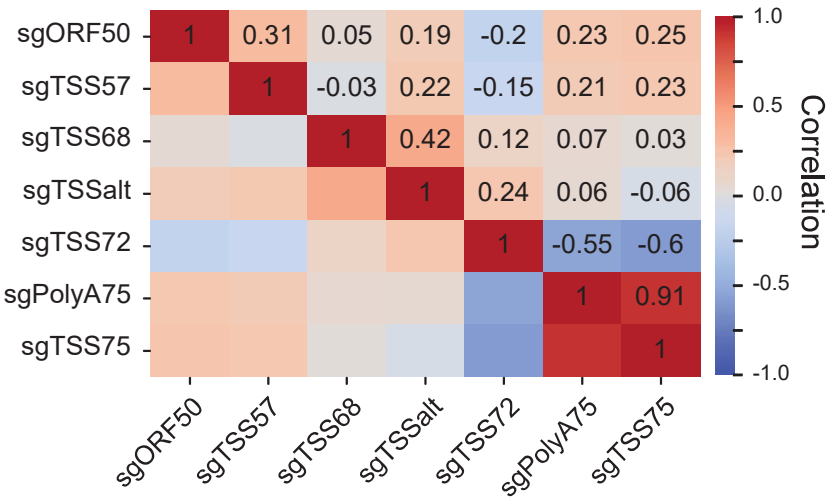
sgORF50
sgTSS57
sgTSS68
sgTSSalt
sgTSS72
sgPolyA75
sgTSS75
1 0.31 0.05 0.19 -0.2 0.23 0.25
1 -0.03 0.22 -0.15 0.21 0.23
1 0.42 0.12 0.07 0.03
1 0.24 0.06 -0.06
1 -0.55 -0.6
1 0.91
1
1.0
0.5
0.0
-0.5
-1.0
Correlation

C

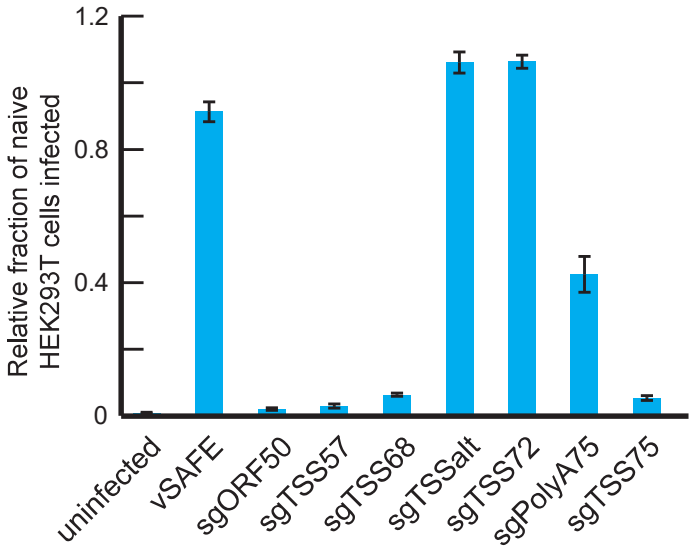
Relative fraction of naive HEK293T cells infected
1.2
0.8
0.4
0
uninfected
vSAFE
sgORF50
sgTSS57
sgTSS68
sgTSSalt
sgTSS72
sgPolyA75
sgTSS75

B

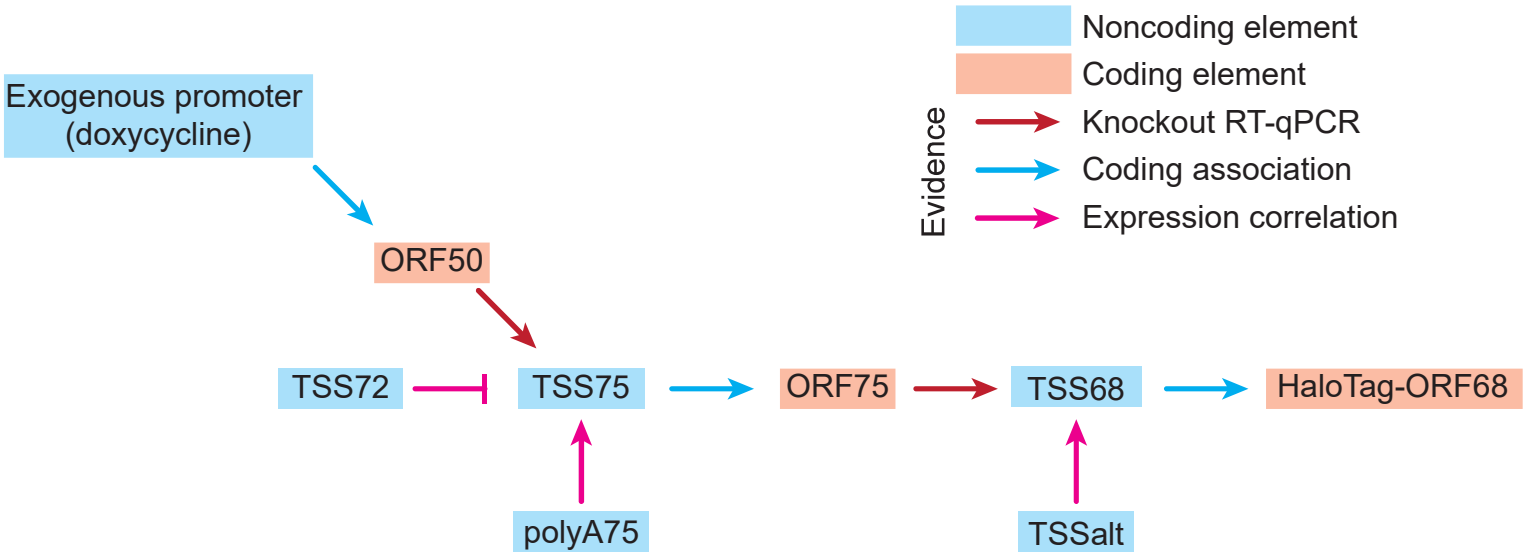
Noncoding element
Coding element
Evidence
Knockout RT-qPCR
Coding association
Expression correlation
Exogenous promoter (doxycycline)
ORF50
TSS72
TSS75
ORF75
TSS68
HaloTag-ORF68
polyA75
TSSalt

Figure S4

A

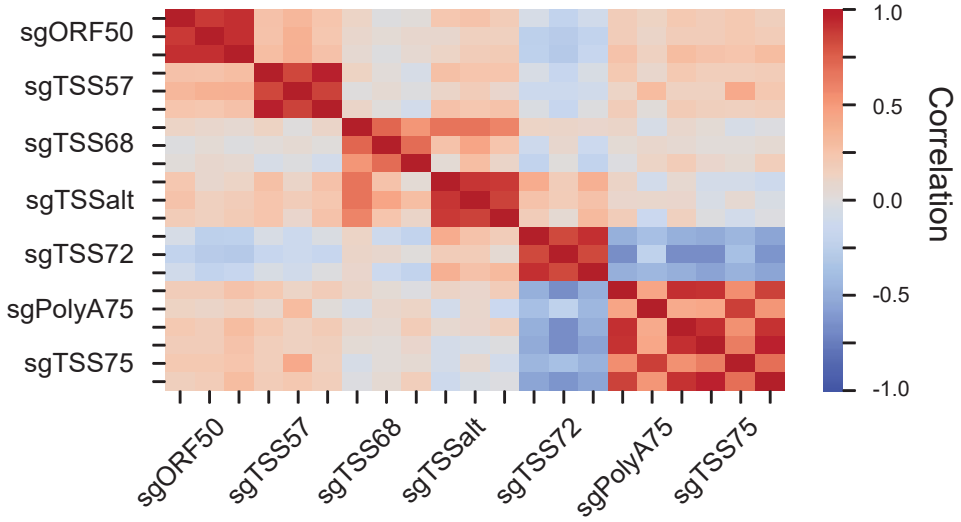
sgORF50
sgTSS57
sgTSS68
sgTSSalt
sgTSS72
sgPolyA75
sgTSS75
1.0
0.5
0.0
-0.5
-1.0
Correlation

Figure 5

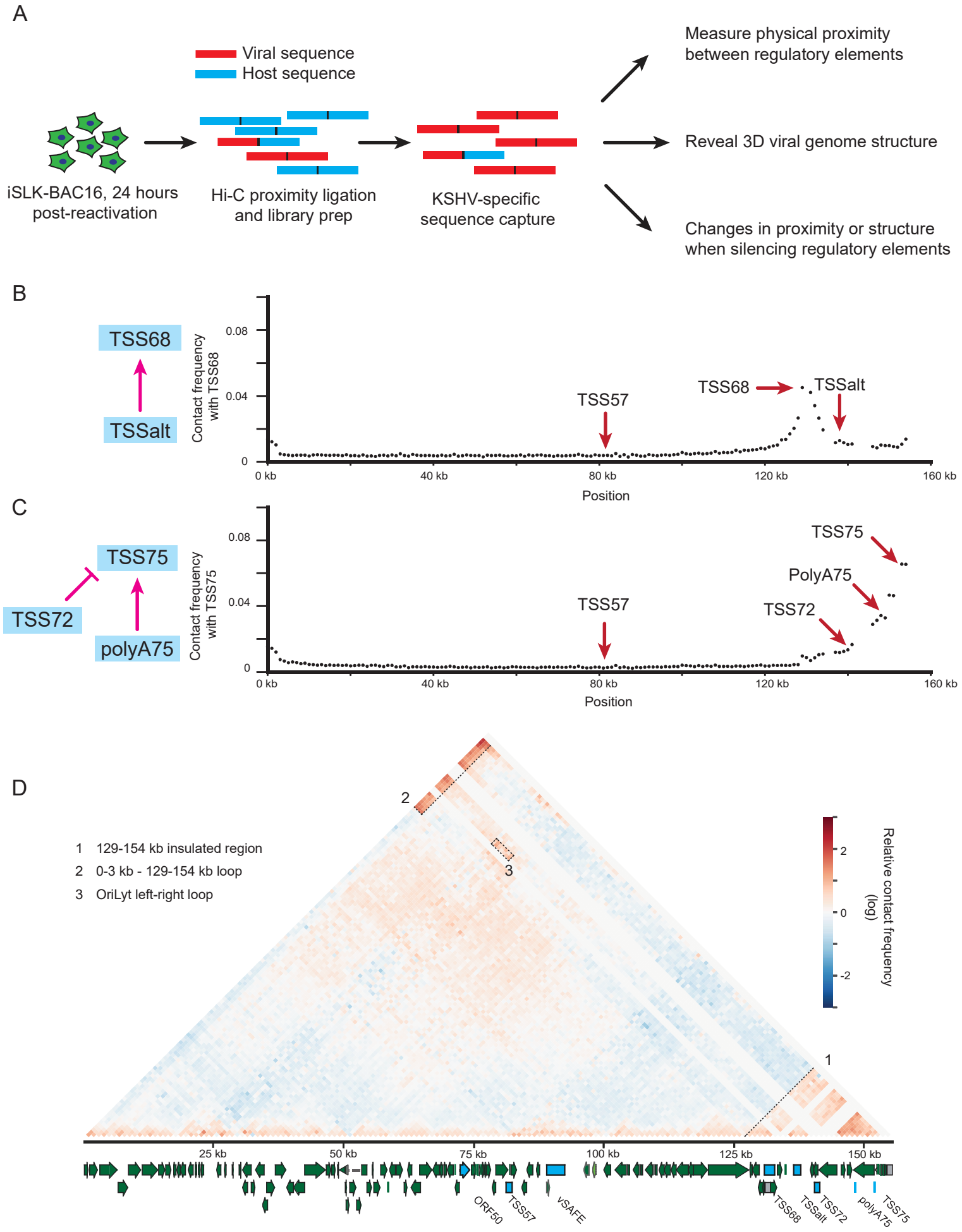
A
Viral sequence
Host sequence
iSLK-BAC16, 24 hours post-reactivation
Hi-C proximity ligation and library prep
KSHV-specific sequence capture
Measure physical proximity between regulatory elements
Reveal 3D viral genome structure
Changes in proximity or structure when silencing regulatory elements
B
TSS68
TSSalt
Contact frequency with TSS68
0.08
0.04
0
TSS57
TSS68
TSSalt
0 kb
40 kb
80 kb
120 kb
160 kb
Position
C
TSS75
TSS72
polyA75
Contact frequency with TSS75
0.08
0.04
0
TSS75
PolyA75
TSS57
TSS72
0 kb
40 kb
80 kb
120 kb
160 kb
Position
D
1 129-154 kb insulated region
2 0-3 kb - 129-154 kb loop
3 OriLyt left-right loop
Relative contact frequency (log)
2
0
-2
25 kb
50 kb
75 kb
100 kb
125 kb
150 kb
ORF50
TSS57
vSAFE
TSS68
TSSalt
TSS72
polyA75
TSS75

Figure S5

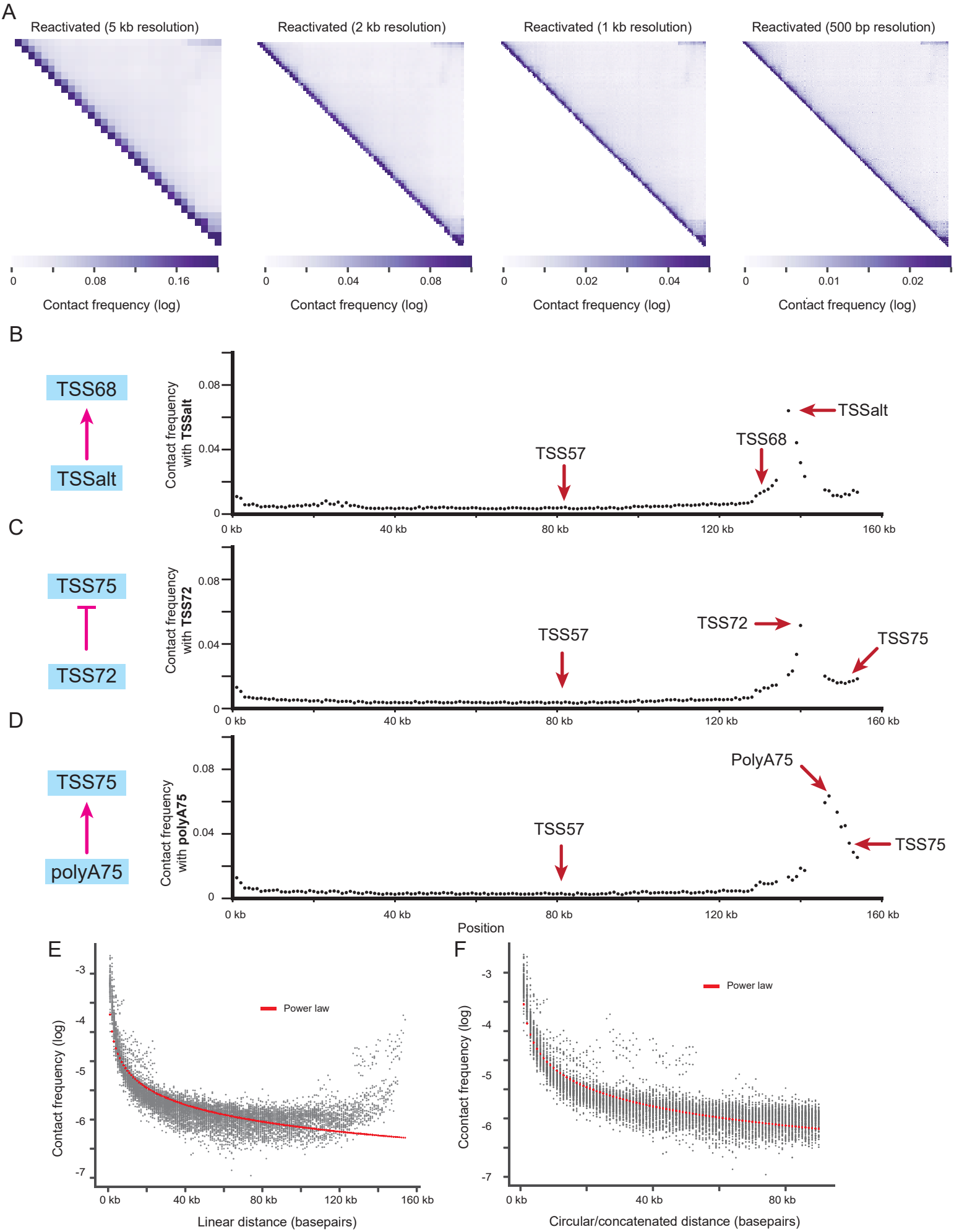
A
Reactivated (5 kb resolution)
Reactivated (2 kb resolution)
Reactivated (1 kb resolution)
Reactivated (500 bp resolution)
0
0.08
0.16
0.04
0.02
0.01
Contact frequency (log)
B
TSS68
TSSalt
Contact frequency with TSSalt
TSS57
TSS68
TSSalt
C
TSS75
TSS72
Contact frequency with TSS72
TSS57
TSS72
TSS75
D
TSS75
polyA75
Contact frequency with polyA75
TSS57
PolyA75
TSS75
0 kb
40 kb
80 kb
120 kb
160 kb
Position
E
Contact frequency (log)
Power law
Linear distance (basepairs)
F
Ccontact frequency (log)
Power law
Circular/concatenated distance (basepairs)

Figure 6

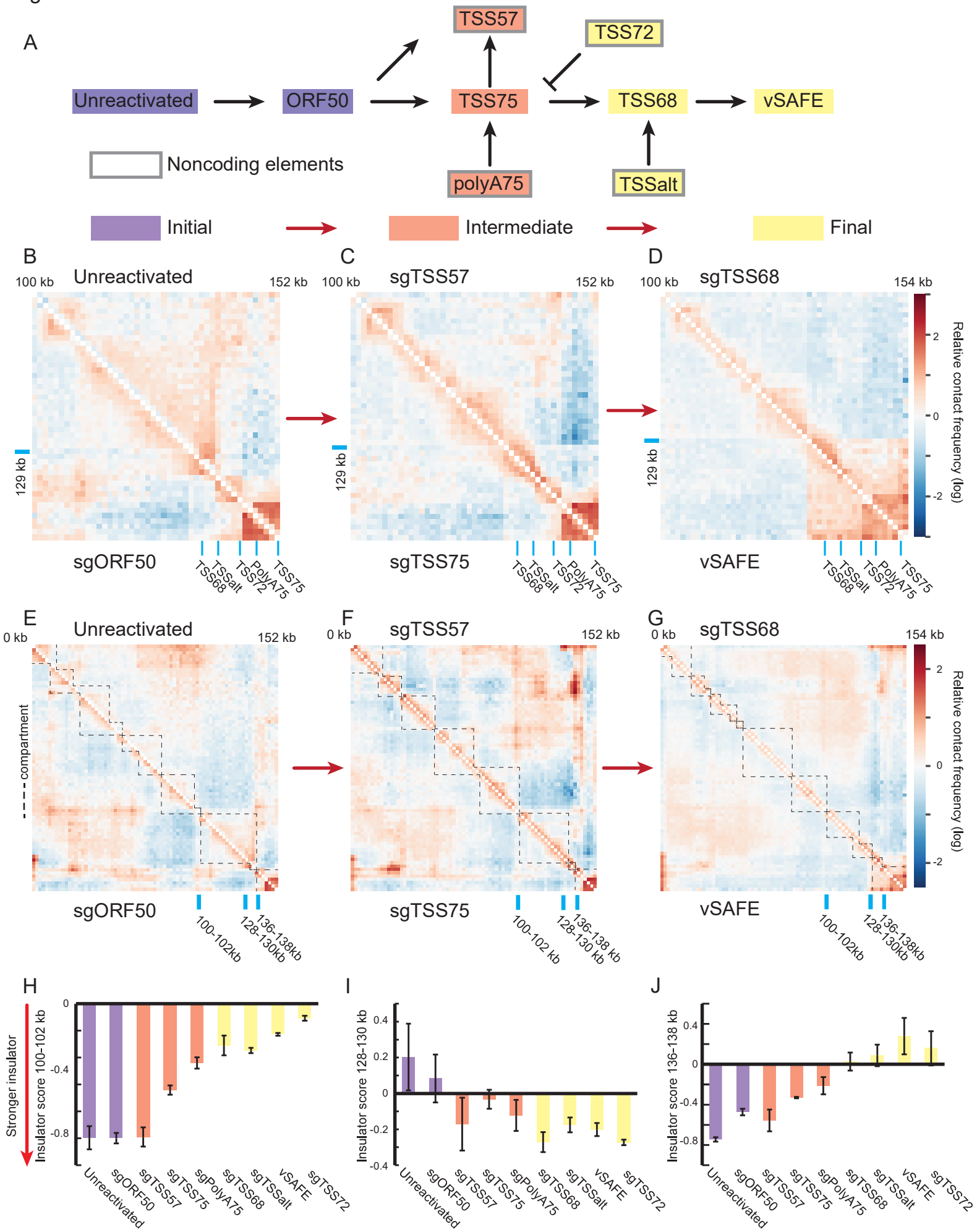
A
TSS57
TSS72
Unreactivated
ORF50
TSS75
TSS68
vSAFE
Noncoding elements
polyA75
TSSalt
Initial
Intermediate
Final
B
Unreactivated
100 kb
152 kb
129 kb
sgORF50
TSS68
TSSalt
TSS72
PolyA75
TSS75
C
sgTSS57
100 kb
152 kb
129 kb
sgTSS75
TSS68
TSSalt
TSS72
PolyA75
TSS75
D
sgTSS68
100 kb
154 kb
129 kb
vSAFE
TSS68
TSSalt
TSS72
PolyA75
TSS75
Relative contact frequency (log)
2
0
-2
E
Unreactivated
0 kb
152 kb
compartment
sgORF50
100-102kb
128-130kb
136-138kb
F
sgTSS57
0 kb
152 kb
sgTSS75
100-102 kb
128-130 kb
136-138 kb
G
sgTSS68
0 kb
154 kb
vSAFE
100-102kb
128-130kb
136-138kb
Relative contact frequency (log)
2
0
-2
H
Stronger insulator
Insulator score 100-102 kb
0
-0.4
-0.8
Unreactivated
sgORF50
sgTSS57
sgTSS75
sgPolyA75
sgTSS68
sgTSSalt
vSAFE
sgTSS72
I
Insulator score 128-130 kb
0.4
0.2
0
-0.2
-0.4
Unreactivated
sgORF50
sgTSS57
sgTSS75
sgPolyA75
sgTSS68
sgTSSalt
vSAFE
sgTSS72
J
Insulator score 136-138 kb
0.4
0
-0.4
-0.8
Unreactivated
sgORF50
sgTSS57
sgTSS75
sgPolyA75
sgTSS68
sgTSSalt
vSAFE
sgTSS72

Figure S6

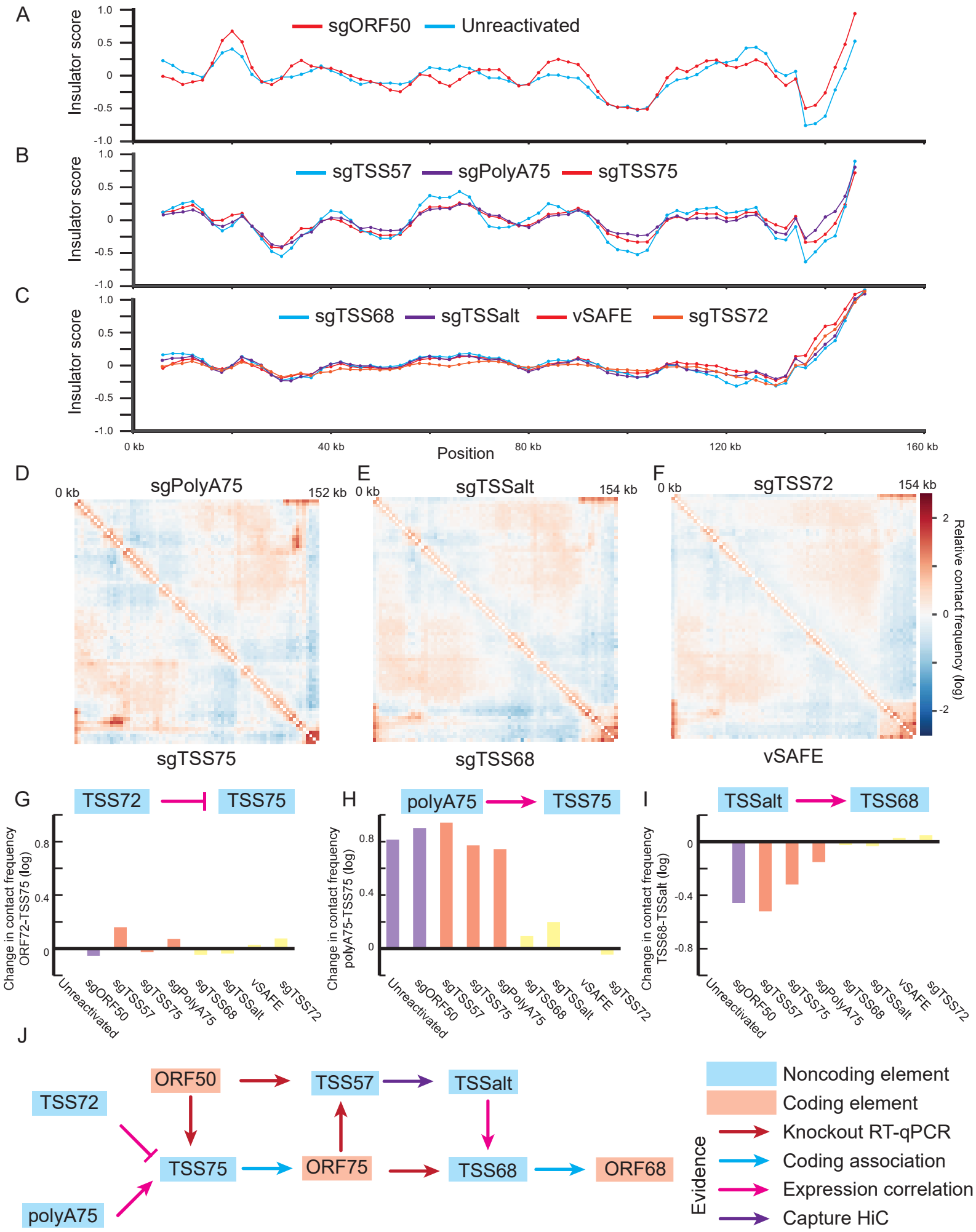
A
Insulator score
sgORF50
Unreactivated
B
sgTSS57
sgPolyA75
sgTSS75
C
sgTSS68
sgTSSalt
vSAFE
sgTSS72
0 kb
40 kb
80 kb
120 kb
160 kb
Position
D
sgPolyA75
152 kb
sgTSS75
E
sgTSSalt
154 kb
sgTSS68
F
sgTSS72
154 kb
vSAFE
Relative contact frequency (log)
G
TSS72
TSS75
Change in contact frequency ORF72-TSS75 (log)
H
polyA75
TSS75
Change in contact frequency polyA75-TSS75 (log)
I
TSSalt
TSS68
Change in contact frequency TSS68-TSSalt (log)
Unreactivated
sgORF50
sgTSS57
sgTSS75
sgPolyA75
sgTSS68
sgTSSalt
vSAFE
sgTSS72
J
TSS72
ORF50
TSS57
TSSalt
TSS75
ORF75
TSS68
ORF68
polyA75
Noncoding element
Coding element
Evidence
Knockout RT-qPCR
Coding association
Expression correlation
Capture HiC

391 **Figure legends**

392 *Figure 1. CRISPRi screen identifies novel viral regulatory regions*. A) Schematic of screen. The
393 viral genome encodes a constitutive fluorescent marker (green) and a HaloTag-ORF68 fusion
394 (blue). B) Summary of results from the CRISPRi screen. X-axis identifies the genome coordinate
395 on the BAC16 KSHV genome. y-axis represents the log-transformed p-value of each locus
396 relative to negative control distribution. Red dotted lines indicate the location of transcriptional
397 start sites. Blue dotted line identifies the two peaks that do not associate with a TSS. C) Validation
398 of pooled guides targeting each peak. Three guides were used to target each locus identified on
399 the x-axis. Y-axis displays the relative percent of cell expressing the HaloTag-ORF68 for the 24
400 or 48 hour post lytic reactivation time points. Error bars represent standard error of four replicates
401 from independent reactivations. D) Enrichment of individual guides at the ORF68 locus. Each dot
402 represents a single guide, with the target location displayed on the x-axis and the average
403 enrichment from two replicates on the y-axis. Arrows represent coding regions of ORF68 (in blue)
404 and surrounding genes in grey.

405 *Figure S1. Supplementary screen data.* A) Enrichment of individual guides at the ORF68 locus.
406 Each dot represents a single guide, with the target location displayed on the x-axis and the
407 average enrichment from two replicates on the y-axis. B) Reproducibility of guide enrichments
408 from two replicates. C-H) Smoothed enrichment of guides at indicated locus with annotated
409 transcription start sites[35]. For each guide, the median enrichment of a 100 bp window centered at
410 the target locus was calculated along with an interquartile range (IQR) to represent the range of
411 values. Median value is shown as a point and IQR is shown as shaded region. Regions significant
412 ($p<10^{-11}$) in sliding window analysis are shown in blue. NA indicates unannotated TSSs.

413 *Figure 2. Local effects caused by CRISPRi*. A) Heat map of changes to viral gene expression at
414 24 hours relative to vSAFE negative controls, with ORF68 presented at the top. Each column
415 shows relative gene expression changes following CRISPRi-induced suppression of the indicated
416 locus. Values are sorted by the effect of sgTSS75. Average of three replicates. B-D) Change in
417 RNA-level of each viral gene relative to vSAFE negative controls in genome-order. Genes whose
418 start codons are within 2.5 kb of at least one guide in targeting pool are highlighted. E) Nascent
419 RNA expression was measured by RT-qPCR at 24 hours post-reactivation from cells treated for
420 two hours with EU. Values are presented relative to parental cells, and error bars are standard
421 error from three independent replicates.

422 *Figure S2*. *Supplementary for RNA-seq*. A) Schematic showing set-up of RNA-seq experiment on
423 CRISPRi cells infected with a three-guide pool, reactivated, and polyA+ RNA-seq at 24 hours
424 post-reactivation. B) Heatmap indicating viral gene expression relative to the matched vSAFE
425 replicate of each individual replicate. Rows are presented in genome order. Replicates from three
426 independent reactivations. C) RT-qPCR was used to measure how CRISPRi-based repression of
427 the individual elements indicated on the x-axis influenced the levels of ORFs 50, 75, 68 and 57
428 mRNA. Error bars represent standard error of four independent reactivations. D) Effect on latency
429 measured by loss of virally encoded EGFP expression over 10 days. Values are presented relative
430 to parental cells, and error bars are standard error from three parallel replicates. P-values are
431 calculated by t-test.

432 *Figure 3. Knockout screen maps associated coding regions*. A-C) Median smoothed enrichments
433 from Cas9 nuclease screen at associated coding locus. Dotted lines indicate exon boundaries.
434 For each guide, the median enrichment of 500 bp window centered at the target locus was
435 calculated along with an IQR. Median value is shown as a point and IQR is shown as shaded
436 region. Regions were considered significant if the guides on each side of the boundary were
437 significantly different and in consistent directions. D) Percent of cells expressing HaloTag-ORF68
438 24 hours post-reactivation for the indicated pool of coding region-targeting guides. Values are
439 averages of four independent replicates and error bars represent standard error. E) RT-qPCR
440 measurements of ORF68, ORF50, ORF75 and ORF57 mRNA at 24 hours post-reactivation
441 following Cas9-based targeting of the loci indicated on the x-axis. Data are presented relative to
442 18S RNA and vSAFE. Error bars show standard error from four technical replicates. F) Average
443 fluorescence from HEK293T cells transfected with an ORF68-promoter-driven HaloTag and a
444 plasmid expressing the indicated viral protein. Error bars are standard error from seven
445 independent replicates.

446 *Figure S3. Coding screen supplement*. A) Enrichment of individual guides. Each dot represents a
447 single guide, with the target location displayed on the x-axis and the average enrichment from
448 two replicates on the y-axis. Red and blue dotted lines represent the median guide enrichment
449 for the two regions indicated. B-D) Median smoothed data from coding screen at indicated locus.
450 For each guide, the median enrichment of a 500 bp window centered at the target locus was
451 calculated along with an IQR. Median value is shown as a point and IQR is shown as shaded
452 region. B) For the EGFP-HygroR locus, location of functional units is shown in color. C,D) Exon
453 boundaries are marked by a dotted line.

454 *Figure 4. Mapping regulatory network by effect on viral transcription*. A) Co-correlation matrix of
455 the RNA-seq data from **Figure 2a**. For each indicated pair of sgRNA pools, a Pearson correlation
456 was calculated between the viral RNA levels. B) Model of regulatory events controlling
457 transcription of the ORF68 locus. C) Supernatant transfer assay measuring changes in KSHV
458 virion production after knockdown of the indicated loci. Error bars represent standard error from
459 six independent reactivations.

460 *Figure S4. Supplementary mapping data.* A) Individual replicate correlation among RNA-seq.

461 *Figure 5. Capture Hi-C of the KSHV genome*. A) Schematic of capture Hi-C experiment. B,C)
462 Contact frequency between B) TSS68 and C) TSS75 and other locations in the viral genome at 1
463 kb resolution. D) Relative contact frequency map corrected for circular/concatenated distance.
464 Noted features are marked and labeled. Positive values represent more interaction than expected.
465 Annotated viral genome is provided with regulatory elements identified marked in blue.

466 *Figure S5. Hi-C data supplement.* A) Contact frequency of reactivated sample at 5 kb, 2 kb, 1 kb,
467 and 500 bp resolution. B-D) Contact frequency between B) TSSalt, C) TSS72, and D) polyA75
468 and other locations in the viral genome at 1 kb resolution. E,F) Observed relationship between
469 observed contact frequency and distance between regions when calculated using E) a linear
470 distance metric or F) a circular/concatenated distance metric.

471 *Figure 6. Changing physical relationship between regulatory regions.* A) Schematic splitting the
472 regulatory network into initial, intermediate, and final stages. B-D) Relative contact frequency at
473 1 kb resolution from 100-154 kb measured by capture Hi-C 24 hours post-reactivation for
474 representative B) initial stages (purple), C) intermediate stages (orange), D) and final stages
475 (yellow). Positive values indicate greater interaction than expected, and locations of regulatory
476 elements are marked in blue. E-G) Relative contact frequency at 2 kb resolution across the
477 genome measured by capture Hi-C 24 hours post-reactivation for representative E) initial stages,
478 F) intermediate stages, G) and final stages. Dotted lines represent locations of insulator regions
479 as defined by negative local-minimum insulator scores. The locations of three observed insulators
480 are marked in blue. H-J) Insulator scores at the marked locations in A-C at D) 100-102 kb, E) 130-
481 132 kb, and F) 136-138 kb. More negative values indicated a stronger insulator. Values are the
482 average of two adjacent regions with error bars representing standard deviation of these two
483 values.

484 *Figure S6. Structural changes supplement*. A-C) Insulator scores for marked conditions
485 measuring the relative frequency of reads crossing a given location. A more negative value

486 indicates a strong insulator. Local minima were used to define the regions marked in **Figure 6e-**
487 **g**. D-F) Relative contact frequency at 2 kb resolution for D) sgPolyA75 and sgTSS75, E) sgTSSalt
488 and sgTSS68, and F) sgTSS72 and vSAFE samples. Positive values indicate greater interaction
489 than expected. G-I) Change in contact frequency from reactivated cells between G) TSS72 and
490 TSS75, H) polyA75 and TSS75, and I) TSS68 and TSSalt at 2 kb resolution. J) Final model for
491 regulatory circuit based on all available data.

492

493 **Methods**

494 *Plasmid and oligos*

495 pMD2.G (Addgene plasmid # 12259), pMDLg/pRRE (Addgene plasmid # 12251) and pRSV-Rev
496 (Addgene plasmid # 12253) were gifts from Didier Trono. pMCB320 was a gift from Michael Bassik
497 (Addgene plasmid # 89359). lentiCas9-Blast was a gift from Feng Zhang (Addgene plasmid #
498 52962). Lenti-dCas9-KRAB-blast was a gift from Gary Hon (Addgene plasmid # 89567).
499 Sequences used are listed in **Supplementary Data 6**.

500 *Cell culture and plasmids*

501 iSLK[55] and Lenti-X 293T (Takara) cells were maintained in DMEM (Gibco +glutamine, +glucose,
502 -pyruvate) with pen-strep (Gibco; 100 I.U./mL) and 1X Glutamax (Gibco) along with 10% FBS
503 (Peak Serum). iSLK cells were maintained in 1 ug/mL puromycin, 50 ug/mL G418, and 125 ug/mL
504 hygromycin B (Gibco). Cas9+ and CRISPRi+ cells were additionally maintained in 10 ug/mL
505 blasticidin. 0.05% Trypsin (Gibco) was used to passage cells. All cells were maintained at 37C
506 and 5% CO2 in a humidity-controlled incubator. Lenti-X 293T cells were obtained from the UCB
507 Cell Culture Facility.

508 *Generation of CRISPRi Halo-ORF68 iSLK line*

509 iSLK cells latently infected with a copy of BAC16[56] containing a HaloTag-ORF68 fusion at the
510 endogenous locus were lentivirally infected with dCas9-KRAB (CRISPRi). Briefly, Lenti-X cells
511 were transfected with third-generation lentiviral mix (pMDLg/pRRE, pRSV-REV, pMD2.G) and
512 dCas9-KRAB (blastR) with polyethylimine (Polysciences). Supernatant was harvested at 48 and
513 72 hours and 0.45 um filtered before applying to iSLK cells for 48 hours. This process was then
514 repeated to ensure high CRISPRi expression.

515 *CRISPRi screening and analysis*

516 A library of guides tiling the KSHV BAC16 genome was delivered lentivirally to the CRISPRi+
517 iSLK cells above. Four days later cells were reactivated with 5 ug/mL doxycycline and 1 mM
518 sodium butyrate and treated with 10 nM JF646 Haloligand (Promega). 24 hours post reactivation,
519 cells were fixed in 4% PFA, and sorted for high and low ORF68 expression using a BD Aria II.
520 Cells were then unfixed overnight in 150 mM NaCl and 60C and 50 ug/mL protease K (Promega).
521 DNA was then extracted using a single column of QIAamp DNA Blood Mini Kit (Qiagen), following
522 the manufacturers' protocol and adjusting initial reaction volume. The sgRNA locus was then
523 amplified and library adaptors ligated as previously described[57]. Libraries were sequenced on an
524 Illumina NovaSeq 6000.

525 Counts for individual guides were converted to enrichment scores by calculating the log2 ratio of
526 counts between high and low populations relative to the median negative control. Enrichment
527 values from two replicates were averaged. To calculate significance of a given window, a 500 bp
528 sliding window was used, comparing the enrichment of each guide and a 500 bp neighborhood
529 to the enrichment scores of all negative controls using a Mann-Whitney test. An arbitrary p-value
530 cutoff was used to identify peaks.

531 *Individual guide delivery*

532 For each pool of sgRNAs, independent lentiviruses were produced as above, then pooled and
533 applied to CRISPRi-positive HaloTag-ORF68 iSLK cells for 48 hours. For protein analysis, cells
534 were reactivated in the presence of 10 nM JF646 Haloligand (Promega) with doxycycline and
535 sodium butyrate as above. Cells were then analyzed for fluorescence at 24 and 48 hours post-
536 reactivation from four independent reactivations on a BD Accuri C6 plus.

537 For latency analysis, cell lines were maintained in triplicate with blasticidin, puromycin, and G418
538 but in the absence of hygromycin. Cells were split every 48 hours and GFP levels were measured
539 by a BD Accuri C6 plus. The percent of GFP positive cells on day 11 was normalized to the percent
540 positive on day 1, and this ratio was again normalized to the loss of GFP observed in parental
541 cells without a guide RNA.

542 *RNA-seq and analysis*

543 RNA samples from above were sent for library preparation and sequencing at the QB3-Berkeley
544 Genomics core labs (RRID:SCR_022170). Total RNA quality as well as poly-dT enriched mRNA
545 quality were assessed on an Agilent 2100 Bioanalyzer. Libraries were prepared using the KAPA
546 RNA Hyper Prep kit (Roche KK8581). Truncated universal stub adapters were ligated to cDNA

547 fragments, which were then extended via PCR using unique dual indexing primers into full length
548 Illumina adapters. Library quality was checked on an AATI (now Agilent) Fragment Analyzer.
549 Library molarity was measured via quantitative PCR with the KAPA Library Quantification Kit
550 (Roche KK4824) on a BioRad CFX Connect thermal cycler. Libraries were then pooled by molarity
551 and sequenced on an Illumina NovaSeq 6000 S4 flowcell for 2 x 150 cycles, targeting at least
552 25M reads per sample. Fastq files were generated and demultiplexed using Illumina bcl_convert
553 and default settings, on a server running CentOS Linux 7.

554 Sequencing quality was assessed with MultiQC and reads were preprocessed with HTStream
555 version 1.3.0 including deduplication. Genome indices were prepared using STAR 2.7.1a. The
556 human GRCh38.p13 genome assembly was indexed with Gencode v43 annotations. Due to
557 overlapping transcripts on the KSHV-BAC16 genome, individual exon coordinates were assigned
558 to the corresponding parent transcript. Preprocessed reads were then aligned using STAR and
559 counts files were generated for transcripts. Any transcript with no reads in all replicates and
560 conditions was eliminated from further analysis. Reads from *E.coli* genes on the BAC were also
561 removed. Raw viral counts were normalized to total input reads for each sample and subsequently
562 normalized to within replicate vSafe condition values. Correlations and heatmaps were generated
563 using the matplotlib, pandas, and seaborn packages in Spyder 5.3.3.

564 *RT-qPCR and EU-RT-qPCR*

565 For RT-qPCR analysis, RNA was extracted at 24 hours post-reactivation using a RNeasy Plus
566 Micro kit (Qiagen), treated with DNAase I (Lucigen), and reverse transcribed using AMV RT
567 (Promega) and random 9-mers in the presence of RNasin (Promega). qPCR was then performed
568 on a Quantstudio 3 using the indicated targets and with iTaq Universal SYBR Green (BioRad).
569 RQ values were calculated using a standard curve. Results are from four independent
570 reactivations.

571 For nascent RNA measurements, cells were reactivated, and 24 hours post-reactivation were
572 treated with 200 uM 5-ethynyl uridine (EU) for two hours. RNA was then extracted using the
573 RNeasy Micro Plus Kit (Qiagen) and EU incorporated RNA was labeled and purified per the Click-
574 iT™ Nascent RNA Capture Kit (Invitrogen). Reverse-transcription was performed on-bead using
575 SuperScript™ VILO™ cDNA Synthesis Kit (Thermo) reverse transcriptase, and qPCR was
576 performed with iTaq Universal SYBR Green (BioRad) or PowerUp™ SYBR™ Green Master Mix
577 (Thermo) on a Quantstudio 3 (Thermo). Relative quantities were calculated using a standard
578 curve. Results are from three independent reactivations.

579 *CRISPR nuclease screen and analysis*

580 Cas9 screen was performed as the CRISPRi screen above using a Cas9+ iSLK cell line infected
581 with a copy of BAC16 containing a HaloTag-ORF68 fusion. The library was then amplified using
582 staggered primers[58] and a modified amplification protocol previously described.[59] qPCR was used
583 to determine cycle number at ¼ CT. All PCR product was run over a single Minelute column
584 (Qiagen) for each sample. Size selection was performed using a gel extraction (Thermo). Library
585 was sequenced on Illumina NextSeq 2000 with a 150bp single-read using Illumina sequencing
586 primers. Adaptors were removed using cutadapt,[60] and reads were aligned to library using
587 bowtie.[61]

588 Log2 values were calculated as above, and enrichment values were averaged from two replicates.
589 For each exon boundary, a window of 500 bp on one side was tested against a 500 bp on the
590 other to calculate p-values using the Mann-Whitney test. Median values were used to determine
591 the sign of the shift. Exons with p values < 0.001 and consistent signs were considered hits.

592 *Transfection of ORF68 reporter*

593 HEK293T cells were transfected using PolyJet In Vitro DNA Transfection Reagent (SignaGen)
594 with a plasmid containing 240 basepairs upstream of ORF68's start codon[32] driving a HaloTag.
595 Cells were cotransfected with either a plasmid expressing ORF75 or ORF50. 24 hours later, cells
596 were treated with JF646 Halo Ligand (Promega) for 24 hours before analysis on a BD Accuri C6
597 plus. Cells were then gated for JF646 signal, and the average fluorescence for the 646 positive
598 cells was calculated. Data are from seven independent replicates.

599 *Supernatant transfer*

600 Cells were reactivated with 5 ug/mL doxycycline and 1 mM sodium butyrate. 72-hour post
601 reactivation, supernatant was filtered through a 0.45 um PES filter and applied to naïve HEK293T
602 cells for 24 hours. HEK cells were then counted on a Accuri C6 Plus (BD) and percent GFP
603 positive was used to calculate infection.

604 *BAC16-specific Capture Hi-C*

605 Capture Hi-C data was generated using the Arima-HiC+ kit, a custom Arima panel specific to the
606 BAC16 KSHV genome, and the Arima Library Prep Module according to the Arima Genomics
607 manufacturer's protocols. Briefly, 24 hours post reactivation, cells were fixed in 4% PFA and
608 frozen. Chromatin was then purified, digested, and filled-in with biotin-labeled nucleotides.
609 Proximity ligation was performed, DNA was purified and sheared, and ligated molecules were

610 enriched by biotin pulldown. Library preparation was then performed, and viral-specific sequences
611 were enriched using capture probes. Libraries were then sequenced using a NextSeq 2000 P2
612 150PE kit (Illumina).

613 *Capture Hi-C analysis*

614 Ditags for Hi-C analysis were aligned to the BAC16 KSHV genome including the HaloTag insertion
615 and filtered using HiCUP version 0.8.0[62] and converted to fragment level counts using CHICACO
616 bam2chicago.[63] Fragments corresponding to the terminal repeats were removed before analysis.
617 The viral genome was then split into bins of 0.5 – 5 kb, and each fragment was assigned to a bin
618 based on the center of the fragment. Each bin was removed if it had less than a total of 5000
619 associated ditags. Bin level counts were then normalized to a symmetric stochastic matrix to
620 calculate contact frequencies by iterative normalization of both rows and columns (Sinkhorn-
621 Knopp). Distance to contact frequency relationship was then graphed using a linear distance
622 metric, and a power law was fit. A second distance metric assuming a circular or concatenated
623 genome was then used, allowing for a 180 kb genome size including ~30 terminal repeats; if the
624 linear distance was greater than half the genome size, then the genome size minus the linear
625 distance was used. A power law was fit to this distribution, and relative contact frequencies are
626 represented as the log ratio of the observed vs the expected power law distribution.

627 Insulator scores were calculated using the principles presented in Crane et al 2015.[64] Contact
628 frequencies spanning each region at 6-10 kb were averaged and normalized to the median value
629 across the genome. Local minima of values lower than 0 were used as insulator locations.

630

631 **Supplementary Data**

632 *Supplementary Data 1. CRISPRi count files.* Raw counts for sequencing from CRISPRi screens.

633 *Supplementary Data 2. CRISPRi screen results.* Processed values for CRISPRi screen.

634 *Supplementary Data 3. RNA-seq counts.* Viral counts for RNA-seq.

635 *Supplementary Data 4. Cas9 count files.* Raw counts for sequencing from Cas9 screens.

636 *Supplementary Data 5. Cas9 screen results.* Processed values for Cas9 screens.

637 *Supplementary Data 6. Sequences.* Sequences used.

638 *Supplementary Data 7. Hi-C results*. Binned interaction counts for each condition.

639

640 **Conflict of interest**

641 The authors declare that they have no conflict of interest.

642

643 **Acknowledgments**

644 The authors would like to thank the Xiaowen Mao and the members of the Glaunsinger lab for
645 their feedback and support, and Dr. C. Kimberly Tsui for the stagger primer sequences. Cell lines
646 were obtained from the UCB Cell Culture Facility which is supported by The University of
647 California Berkeley (SCR_017924). RNA-seq was performed by the Berkeley functional genomics
648 core (QB3 Genomics, UC Berkeley, Berkeley, CA, RRID:SCR_022170). Flow cytometry and
649 FACS were conducted at the CRL Flow Cytometry Facility. We thank Hector Nolla and Alma
650 Valeros of the UC Berkeley Cancer Research Laboratory Flow Cytometry Facility for training and
651 expertise. This work used the Vincent J. Coates Genomics Sequencing Laboratory at UC
652 Berkeley, supported by NIH S10 OD018174 Instrumentation Grant. B.A.G. is an investigator of
653 the Howard Hughes Medical Institute, and D.W.M. is a Howard Hughes Medical Institute Awardee
654 of the Life Sciences Research Foundation. This research was also funded by NIH grant
655 K99AI173531 to D.W.M and AI122528 to B.A.G.

656 1. Kutluay, S. B. & Triezenberg, S. J. Role of chromatin during herpesvirus infections.
657 *Biochim. Biophys. Acta* **1790**, 456–66 (2009).

658 2. Toth, Z. *et al.* Epigenetic analysis of KSHV latent and lytic genomes. *PLoS Pathog.* **6**, 1–
659 17 (2010).

660 3. Qi, Y. *et al.* Latency-associated nuclear antigen inhibits lytic replication of Kaposi's
661 sarcoma-associated herpesvirus by regulating let-7a/RBPJ signaling. *Virology* **531**, 69–
662 78 (2019).

663 4. Stedman, W. *et al.* Cohesins localize with CTCF at the KSHV latency control region and
664 at cellular c-myc and H19/Igf2 insulators. *EMBO J.* **27**, 654 (2008).

665 5. Campbell, M. *et al.* KSHV episomes reveal dynamic chromatin loop formation with
666 domain-specific gene regulation. *Nat. Commun. 2017 91* **9**, 1–14 (2018).

667 6. Banerji, J., Rusconi, S. & Schaffner, W. Expression of a β-globin gene is enhanced by
668 remote SV40 DNA sequences. *Cell* **27**, 299–308 (1981).

669 7. Loeken, M. R. & Brady, J. The Adenovirus EIIA Enhancer. *J. Biol. Chem.* **264**, 6572–
670 6579 (1989).

671 8. Stinski, M. F. & Isomura, H. Role of the cytomegalovirus major immediate early enhancer
672 in acute infection and reactivation from latency. *Med. Microbiol. Immunol.* **197**, 223–231
673 (2008).

674 9. Dooley, A. L. & O'Connor, C. M. Regulation of the MIE Locus During HCMV Latency and
675 Reactivation. **9**, (2020).

676 10. Izumiya, Y. *et al.* Kaposi's sarcoma-associated herpesvirus terminal repeat regulates
677 inducible lytic gene promoters. *J. Virol.* **98**, (2024).

678 11. Feldman, E. R. *et al.* A Gammaherpesvirus Noncoding RNA Is Essential for
679 Hematogenous Dissemination and Establishment of Peripheral Latency. *mSphere* **1**,
680 (2016).

681 12. Hoffman, B. A., Wang, Y., Feldman, E. R. & Tibbetts, S. A. Epstein-Barr virus EBER1 and
682 murine gammaherpesvirus TMER4 share conserved in vivo function to promote B cell
683 egress and dissemination. *Proc. Natl. Acad. Sci. U. S. A.* **116**, 25392–25394 (2019).

684 13. Hu, M. *et al.* A KSHV microRNA Directly Targets G Protein-Coupled Receptor Kinase 2 to

685 Promote the Migration and Invasion of Endothelial Cells by Inducing CXCR2 and
686 Activating AKT Signaling. *PLOS Pathog.* **11**, e1005171 (2015).

687 14. Gay, L. A., Stribling, D., Turner, P. C. & Renne, R. Kaposi's Sarcoma-Associated
688 Herpesvirus MicroRNA Mutants Modulate Cancer Hallmark Phenotypic Differences in
689 Human Endothelial Cells. *J. Virol.* **95**, (2021).

690 15. Wang, Y., Tang, Q., Maul, G. G. & Yuan, Y. Kaposi's sarcoma-associated herpesvirus
691 ori-Lyt-dependent DNA replication: dual role of replication and transcription activator. *J.*
692 *Virol.* **80**, 12171–12186 (2006).

693 16. Wang, Y. *et al.* Kaposi's sarcoma-associated herpesvirus ori-Lyt-dependent DNA
694 replication: cis-acting requirements for replication and ori-Lyt-associated RNA
695 transcription. *J. Virol.* **78**, 8615–8629 (2004).

696 17. Tagawa, T. *et al.* Discovery of Kaposi's sarcoma herpesvirus-encoded circular RNAs and
697 a human antiviral circular RNA. *Proc. Natl. Acad. Sci. U. S. A.* **115**, 12805–12810 (2018).

698 18. Tagawa, T. *et al.* Characterizing Expression and Regulation of Gamma-Herpesviral
699 Circular RNAs. *Front. Microbiol.* **12**, (2021).

700 19. Rossetto, C. C. & Pari, G. S. Kaposi's sarcoma-associated herpesvirus noncoding
701 polyadenylated nuclear RNA interacts with virus- and host cell-encoded proteins and
702 suppresses expression of genes involved in immune modulation. *J. Virol.* **85**, 13290–7
703 (2011).

704 20. Campbell, M. & Izumiya, Y. PAN RNA: transcriptional exhaust from a viral engine. *J.*
705 *Biomed. Sci. 2020 271* **27**, 1–10 (2020).

706 21. Sun, R., Lin, S. F., Gradoville, L. & Miller, G. Polyadenylylated nuclear RNA encoded by
707 Kaposi sarcoma-associated herpesvirus. *Proc. Natl. Acad. Sci. U. S. A.* **93**, 11883–11888
708 (1996).

709 22. Schifano, J. M., Corcoran, K., Kelkar, H. & Dittmer, D. P. Expression of the Antisense-to-
710 Latency Transcript Long Noncoding RNA in Kaposi's Sarcoma-Associated Herpesvirus.
711 *J. Virol.* **91**, (2017).

712 23. Chandriani, S., Xu, Y. & Ganem, D. The Lytic Transcriptome of Kaposi's Sarcoma-
713 Associated Herpesvirus Reveals Extensive Transcription of Noncoding Regions,
714 Including Regions Antisense to Important Genes. *J. Virol.* **84**, 7934 (2010).

715 24. Hilton, I. B. *et al.* Epigenome editing by a CRISPR-Cas9-based acetyltransferase
716 activates genes from promoters and enhancers. *Nat. Biotechnol. 2015 335* **33**, 510–517
717 (2015).

718 25. Thakore, P. I. *et al.* Highly specific epigenome editing by CRISPR-Cas9 repressors for
719 silencing of distal regulatory elements. *Nat. Methods 2015 1212* **12**, 1143–1149 (2015).

720 26. Liu, S. J. *et al.* CRISPRi-based genome-scale identification of functional long noncoding
721 RNA loci in human cells. *Science* **355**, (2017).

722 27. Fulco, C. P. *et al.* Systematic mapping of functional enhancer-promoter connections with
723 CRISPR interference. *Science* **354**, 769 (2016).

724 28. Tycko, J. *et al.* Mitigation of off-target toxicity in CRISPR-Cas9 screens for essential non-
725 coding elements. *Nat. Commun.* **10**, (2019).

726 29. Brackett, K. *et al.* Crispr interference efficiently silences latent and lytic viral genes in
727 kaposi's sarcoma-associated herpesvirus-infected cells. *Viruses* **13**, (2021).

728 30. Gabaev, I., Williamson, J. C., Crozier, T. W. M., Schulz, T. F. & Lehner, P. J. Quantitative
729 Proteomics Analysis of Lytic KSHV Infection in Human Endothelial Cells Reveals Targets
730 of Viral Immune Modulation. *Cell Rep.* **33**, (2020).

731 31. Arias, C. *et al.* KSHV 2.0: A Comprehensive Annotation of the Kaposi's Sarcoma-
732 Associated Herpesvirus Genome Using Next-Generation Sequencing Reveals Novel
733 Genomic and Functional Features. *PLoS Pathog.* **10**, e1003847 (2014).

734 32. Gardner, M. R. & Glaunsinger, B. A. Kaposi's Sarcoma-Associated Herpesvirus ORF68
735 Is a DNA Binding Protein Required for Viral Genome Cleavage and Packaging. *J. Virol.*
736 **92**, (2018).

737 33. Didychuk, A. L. *et al.* A pentameric protein ring with novel architecture is required for
738 herpesviral packaging. *Elife* **10**, 1–31 (2021).

739 34. Morgens, D. W., Nandakumar, D., Didychuk Id, A. L., Yang, K. J. & Glaunsingerid, B. A.
740 A Two-tiered functional screen identifies herpesviral transcriptional modifiers and their
741 essential domains. *PLOS Pathog.* **18**, e1010236 (2022).

742 35. Ye, X., Zhaoid, Y. & Karijolich, J. The landscape of transcription initiation across latent
743 and lytic KSHV genomes. *PLoS Pathog.* **15**, e1007852 (2019).

744 36. Gregory Bruce, A. *et al.* Quantitative Analysis of the KSHV Transcriptome Following
745 Primary Infection of Blood and Lymphatic Endothelial Cells. *Pathog. (Basel, Switzerland)*
746 **6**, (2017).

747 37. Lensch, S. *et al.* Dynamic spreading of chromatin-mediated gene silencing and
748 reactivation between neighboring genes in single cells. *Elife* **11**, (2022).

749 38. Guito, J. & Lukac, D. M. KSHV Rta promoter specification and viral reactivation. *Front.*
750 *Microbiol.* **3**, 30 (2012).

751 39. Komander, D. & Rape, M. The ubiquitin code. *Annu. Rev. Biochem.* **81**, 203–29 (2012).

752 40. McCollum, C. O. *et al.* The viral packaging motor potentiates Kaposi's sarcoma-
753 associated herpesvirus gene expression late in infection. *PLOS Pathog.* **19**, e1011163
754 (2023).

755 41. Majerciak, V. & Zheng, Z. M. KSHV ORF57, a Protein of Many Faces. *Viruses* **7**, 604
756 (2015).

757 42. Uppal, T., Banerjee, S., Sun, Z., Verma, S. C. & Robertson, E. S. KSHV LANA—The
758 Master Regulator of KSHV Latency. *Viruses* **6**, 4961 (2014).

759 43. Campbell, M. *et al.* KSHV Topologically Associating Domains in Latent and Reactivated
760 Viral Chromatin. *J. Virol.* **96**, 14 (2022).

761 44. Kumar, A. *et al.* KSHV episome tethering sites on host chromosomes and regulation of
762 latency-lytic switch by CHD4. *Cell Rep.* **39**, (2022).

763 45. Lieberman-Aiden, E. *et al.* Comprehensive mapping of long-range interactions reveals
764 folding principles of the human genome. *Science* **326**, 289–293 (2009).

765 46. Zhou, Y. *et al.* Modeling and analysis of Hi-C data by HiSIF identifies characteristic
766 promoter-distal loops. *Genome Med.* **12**, 1–13 (2020).

767 47. De Leo, A., Chen, H. S., Hu, C. C. A. & Lieberman, P. M. Deregulation of KSHV latency
768 conformation by ER-stress and caspase-dependent RAD21-cleavage. *PLoS Pathog.* **13**,
769 (2017).

770 48. Kang, H., Wiedmer, A., Yuan, Y., Robertson, E. & Lieberman, P. M. Coordination of
771 KSHV Latent and Lytic Gene Control by CTCF-Cohesin Mediated Chromosome
772 Conformation. *PLOS Pathog.* **7**, e1002140 (2011).

773 49. Campbell, M. *et al.* KSHV episomes reveal dynamic chromatin loop formation with
774 domain-specific gene regulation. *Nat. Commun.* **9**, (2018).

775 50. T, K.-N. *et al.* Overexpression of the kaposi's sarcoma-associated herpesvirus
776 transactivator K-Rta can complement a K-bZIP deletion BACmid and yields an enhanced
777 growth phenotype. *J. Virol.* **81**, 13519–13532 (2007).

778 51. Full, F. *et al.* Kaposi's Sarcoma Associated Herpesvirus Tegument Protein ORF75 Is
779 Essential for Viral Lytic Replication and Plays a Critical Role in the Antagonization of
780 ND10-Instituted Intrinsic Immunity. *PLOS Pathog.* **10**, e1003863 (2014).

781 52. Chowdhury, N. R., Gurevich, V. & Shamay, M. KSHV genome harbors both constitutive
782 and lytically induced enhancers. *bioRxiv* 2024.01.30.577957 (2024)
783 doi:10.1101/2024.01.30.577957.

784 53. Verma, D., Li, D.-J., Krueger, B., Renne, R. & Swaminathan, S. Identification of the
785 Physiological Gene Targets of the Essential Lytic Replicative Kaposi's Sarcoma-
786 Associated Herpesvirus ORF57 Protein. *J. Virol.* **89**, 1688–1702 (2015).

787 54. Chen, P. B. *et al.* Systematic discovery and functional dissection of enhancers needed for
788 cancer cell fitness and proliferation. *Cell Rep.* **41**, 111630 (2022).

789 55. Myoung, J. & Ganem, D. Generation of a doxycycline-inducible KSHV producer cell line
790 of endothelial origin: Maintenance of tight latency with efficient reactivation upon
791 induction. *J. Virol. Methods* **174**, 12–21 (2011).

792 56. Brulois, K. F. *et al.* Construction and Manipulation of a New Kaposi's Sarcoma-
793 Associated Herpesvirus Bacterial Artificial Chromosome Clone. *J. Virol.* **86**, 9708–9720
794 (2012).

795 57. Deans, R. M. *et al.* Parallel shRNA and CRISPR-Cas9 screens enable antiviral drug
796 target identification. *Nat. Chem. Biol.* **12**, 361–366 (2016).

797 58. Tsui, C. K. *et al.* Combinatorial CRISPR screens and lectin microarrays identify novel
798 glycosylation regulators. *bioRxiv* 2023.10.23.563662 (2023)
799 doi:10.1101/2023.10.23.563662.

800 59. Morgens, D. W. *et al.* Retro-2 protects cells from ricin toxicity by inhibiting ASNA1-
801 mediated ER targeting and insertion of tail-anchored proteins. *Elife* **8**, (2019).

802 60. Martin, M. Cutadapt removes adapter sequences from high-throughput sequencing
803 reads. *EMBnet.journal* **17**, 10 (2011).

804 61. Langmead, B., Trapnell, C., Pop, M. & Salzberg, S. L. Ultrafast and memory-efficient
805 alignment of short DNA sequences to the human genome. *Genome Biol.* **10**, R25 (2009).

806 62. Wingett, S. *et al.* HiCUP: pipeline for mapping and processing Hi-C data. *F1000Research*
807 **4**, (2015).

808 63. Cairns, J. *et al.* CHiCAGO: Robust detection of DNA looping interactions in Capture Hi-C
809 data. *Genome Biol.* **17**, 1–17 (2016).

810 64. Crane, E. *et al.* Condensin-driven remodelling of X chromosome topology during dosage
811 compensation. *Nat. 2015 5237559* **523**, 240–244 (2015).

812